

Article

Geochemical and Mineralogical Approaches in Unraveling Paleoweathering, Provenance, and Tectonic Setting of the Clastic Sedimentary Succession (Western Central Paratethys)

Kristina Ivancič^{1,*} , Rok Brajkovič¹  and Mirijam Vrabc ² ¹ Geological Survey of Slovenia, Dimičeva ulica 14, 1000 Ljubljana, Slovenia; rok.brajkovic@geo-zs.si² Department of Geology, Faculty of Natural Sciences and Engineering, University of Ljubljana, Aškerčeva cesta 12, 1000 Ljubljana, Slovenia; mirijam.vrabc@ntf.uni-lj.si

* Correspondence: kristina.ivancic@geo-zs.si

Abstract: Pronounced tectonic and paleogeographic changes were detected in the Alpine–Pannonian region during the Miocene at the interface between the Alps, the Dinarides, and the Pannonian Basin. To understand the major tectonic, paleogeographic, and paleoclimatic changes during this period, geochemical and mineralogical investigations were carried out on the fine-grained clastic sedimentary rocks in the Tunjice Hills. The paleoweathering indicates a cold and/or arid to a warm and humid period. The paleoclimate and the regional climatic conditions correspond well with the Middle Miocene Climatic Optimum. The mineral composition shows an abundance of quartz and calcite. Quartz is associated with detrital origin from volcanic and metamorphic rocks of the Eastern and Southern Alps and with authigenic processes in sediments. Calcite is related to authigenic origin formed in shallow marine environments and to detrital provenance from the Southern Alps. Not all discriminant functions based on major oxides provided adequate results in determining the tectonic setting. The source rocks were subjected to oceanic island arc and collision. Moreover, sedimentation was influenced by both active and passive margin settings. The former is related to the Alpine collision, which continued from the Cenozoic onward, and the latter is connected to the processes associated with the formation of the Pannonian Basin System, which began in the late Early Miocene.

Keywords: Central Paratethys; provenance; tectonic setting; paleoweathering; Miocene; Tunjice Hills



Citation: Ivancič, K.; Brajkovič, R.; Vrabc, M. Geochemical and Mineralogical Approaches in Unraveling Paleoweathering, Provenance, and Tectonic Setting of the Clastic Sedimentary Succession (Western Central Paratethys). *Appl. Sci.* **2024**, *14*, 537. <https://doi.org/10.3390/app14020537>

Academic Editors: Andrea L. Rizzo, Leonid Perelomov, Inna Zamulina and Sudhir S. Shende

Received: 14 November 2023

Revised: 18 December 2023

Accepted: 4 January 2024

Published: 8 January 2024



Copyright: © 2024 by the authors. Licensee MDPI, Basel, Switzerland. This article is an open access article distributed under the terms and conditions of the Creative Commons Attribution (CC BY) license (<https://creativecommons.org/licenses/by/4.0/>).

1. Introduction

The use of major oxides in geochemistry and mineralogical analyses to determine paleoweathering, origin, and tectonic setting is one of the most effective and long-established methods for studying of sedimentary basins for different rock types and sediment ages [1–13]. Over geological time, specific processes, such as tectonic activity, paleoweathering conditions, and variations in drainage systems, changed. These changes are preserved in rocks, and the use of mineralogical and geochemical methods allows us to distinguish differences in paleogeography, climate and tectonic processes in a particular area at a particular time. However, not all provenance determination diagrams are sufficiently precise, and they do not provide compatible results. Caution is also required when using and interpreting different discriminant functions [2,14,15]. In addition, caution should be exercised when interpreting paleoweathering due to the influence of provenance, which itself can be negated by utilizing different models and analyses [16].

The Pannonian Basin System (PBS) represents a large basin within the well-studied Alpine, Carpathian, and Dinaric mountain ranges [17–22] (Figure 1a), with major tectonic, climatic and paleogeographic changes during the Miocene [23,24]. Geochemical and mineralogical approaches are not common in the sedimentary successions of the Miocene sediments of the PBS, with only a few studies focusing on geochemical and mineralogical analyses and the determination of paleoweathering, provenance, tectonic setting, and

paleoenvironment [15,25–28]. The structurally extremely complex evolution and dynamic area of the PBS may be the crux of the matter [21,29–33].

The basement of the PBS consists of two lithospheric blocks—Tisza and Dacia. The movement and rotation of the blocks strongly influenced the evolution of the PBS [18,29,34]. In addition, various tectonic processes influenced the development of the studied area from the Miocene onwards, starting with the collision of the Adriatic and European lithospheric plates, which caused the Alpine orogen, the continental escape of the Eastern Alps, thrusting and folding of the Dinarides, and the syn-rift and post-rift Miocene extensions [20,35,36]. These processes significantly influenced the evolution of faults and the fault system, which in turn affected the evolution of the environment and sediments [37–39].

The evolution of the southwestern PBS was also affected by climate change, especially in the Early and Middle Miocene, which caused changes in depositional environments and sedimentary style. In addition, the temporary isolation of the Central Paratethys from the Mediterranean and Indian Ocean led to limited exchange of fauna from the open ocean, resulting in the development of restricted fossil assemblages. Therefore, a regional chronostratigraphic subdivision was established. It differed from the global stages (Figure 1b), and was primarily based on paleontological criteria [23,24,40–44].

The main objective of this study is to determine the degree of paleoweathering, the main source of sediments, and the main tectonic settings during the period from the beginning of the Early Miocene (Egerian) to the end of the Middle Miocene (Sarmatian), based on mineralogical and geochemical data from the sedimentary successions from the Tunjice Hills (Western Pannonian Basin System, Western Central Paratethys). In addition, we aim to evaluate the reliability of these methods on sediments located at the interface of several tectonic units and possibly subjected to various tectonic processes. To achieve all these objectives, the paper aims to unravel the impact of the main processes that contributed to the changes in the paleogeography that influenced the early cessation of sedimentation and uplift of the western margins of the PBS. Furthermore, the climatic conditions and the relationship between the paleoclimate of the study area and the Miocene Climatic Optimum are discussed.

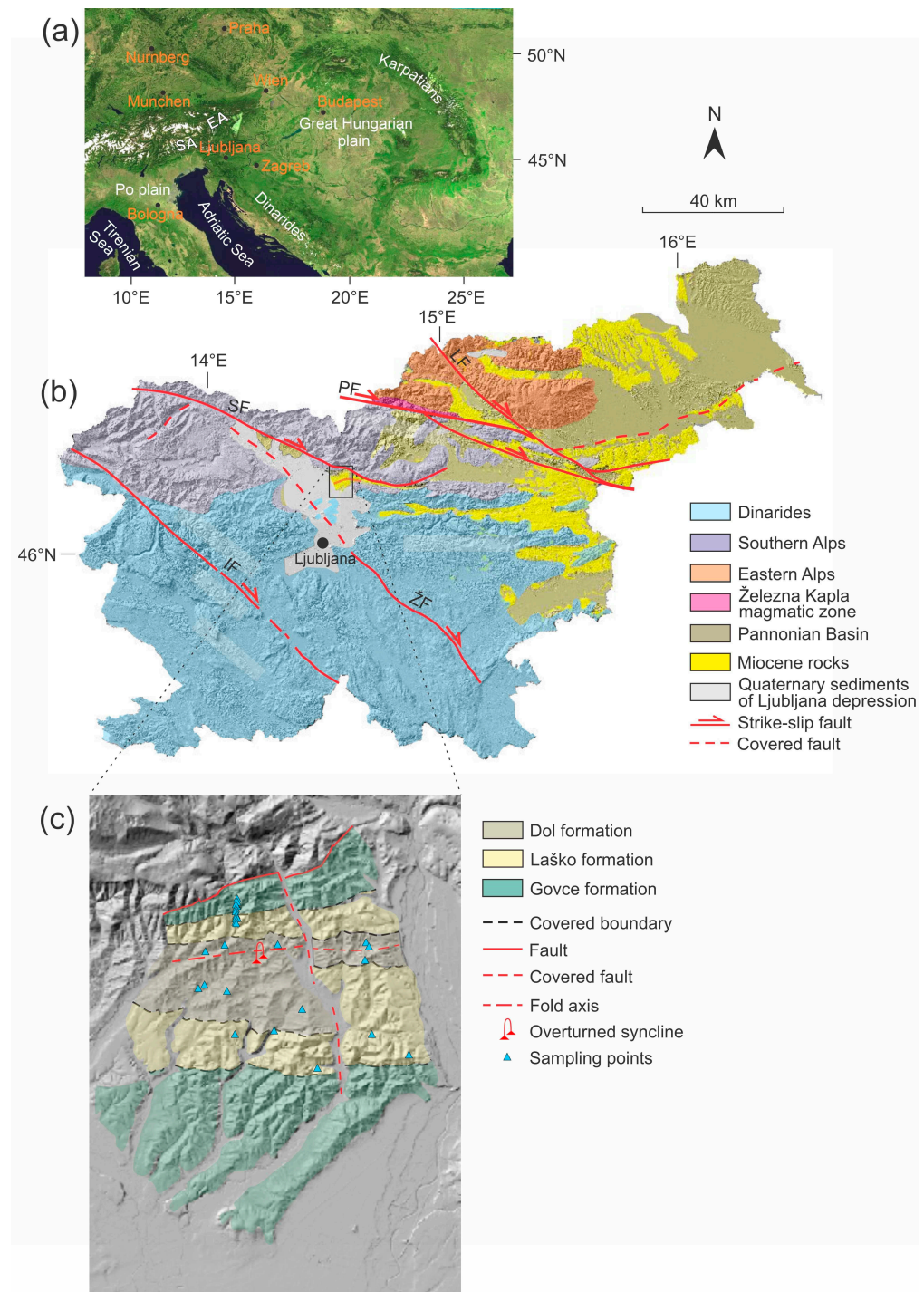


Figure 1. (a) Modified google image of the Alpine–Carpathian–Pannonian region; (b) area of Slovenia with geotectonic units, modified after [45,46], and the spatial distribution of the Miocene rocks; (c) simplified map of the Tunjice Hills, modified after [47,48]. Explanatory notes: SA—Southern Alps, EA—Eastern Alps, SF—Sava Fault, PF—Periadriatic Fault, LF—Labot Fault, ŽF—Žužemberk Fault, IF—Idrija Fault, PG—Paleogene, UM—Upper Miocene, OL—Oligocene, Eggenb—Eggenburgian, D. f.—Dol formation.

2. Geological Setting

The Tunjice Hills are located in the central part of Slovenia (Figure 1a). Structurally, the area represents the western margin of the tectonic unit of the Neogene PBS and is surrounded by the tectonic units of the Southern Alps, Eastern Alps, and the Dinarides. The juncture of these tectonic units with the still-active Sava fault in the north [49] represents a structurally and geodynamically complex area. North of the Tunjice Hills, the Southern Alps consist largely of Triassic carbonate rocks, mainly limestones, and also dolomites, shales, and sandstones with tuffs [50,51]. North of the Southern Alps, the Upper and Lower Austroalpine units of the Eastern Alps occur, consisting of low- to ultrahigh-grade metamorphic rocks [20,52,53]. The units are part of a large ALCAPA mega-unit [19]. The Oligocene volcanic and volcanoclastic rocks of the Smrekovec volcanic complex are located northeast of the Tunjice Hills [54]. To the south, the contact with the Dinarides is covered by Quaternary sediments. The Dinaridic basement consists of clay stones, siltstones, sandstones, and quartz conglomerates of the Carboniferous to the Permian [51], and is overlain by a thick sequence of Mesozoic carbonates [55]. To the west, southwest and southeast, the deeper marine rocks of the Mesozoic occur in the Tolmin nappe [45]. This structural complexity is recorded in the Neogene strata.

The global regressive-transgressive cycles influenced sedimentation in the Tunjice Basin as well, from the Oligocene to the end of the Middle Miocene [51,56]. The Oligocene sedimentary rocks consist of conglomerates and clays [51] and indicate initial Cenozoic sedimentation in the Tunjice Hills in a shallow marine environment [56,57] before the formation of the PBS. Sedimentation continued with deposition of the Early Miocene (Egerian and Eggenburgian stages) conglomerates, sandstones, and marlstones, known as Govce beds, in a brackish and marine environment [51,58], and are rich in fossil remains [57]. The regional distribution of similar Early Miocene deposits indicates the development of the western–southwestern part of a restricted shallow epicontinental sea in the Central Paratethys [59]. Sedimentation is not determined in the late Early Miocene (Ottangian and Karpatian stages), when the evolution of the PBS started. The Badenian transgression [60] also influenced the studied succession in the Middle Miocene, when the Badenian wide-rift extension in the PBS was already in full progress [36]. Marls and sands were deposited, known as the Laško formation [51]. The stable and warm paleoclimatic conditions during the Badenian period led to an expansion of fauna and flora [23,40,61], resulting in the preservation of many marine fossil remains. The Tunjice area share similar characteristics [51,62]. At the end of the Middle Miocene, the Sarmatian strata were represented by marlstone, mudstone, sandstone, and calcarenites, which reflect deposition in a marine environment of reduced salinity, and are known as the Dol formation [51,56]. Younger rocks (upper Miocene to Pleistocene) have not yet been determined in the Tunjice Hills.

The Miocene strata in the Tunjice Hills were deformed during the Miocene by syn-rift and post-rift extensional and compressional processes, which led to the formation of the overturned syncline of Tunjice, with the northern limb in an inverse position [51,56]. Thus, the youngest layers of the Dol formation are located in the center of the syncline (in the central part of the Tunjice Hills), the Middle Miocene layers of the Laško formation are located north and south of the Dol formation and the lower Miocene layers of the Govce formation at the edges of the syncline (north and south of the Tunjice Hills; Figure 2). In addition, the Tunjice Hills are deformed by a dextral strike-slip fault, the so-called Tunjice Fault, in the NNW–SSE direction [47].

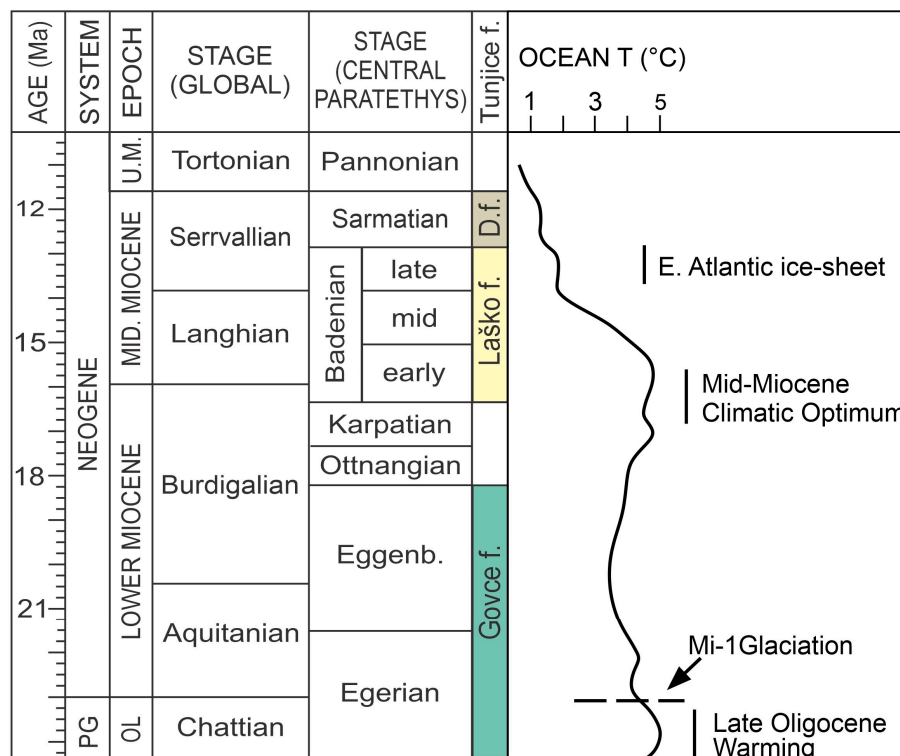


Figure 2. International and Central Paratethys chronostratigraphic chart, modified after [40,43] with added formations in the study area (Tunjice Hills) with ocean temperature curve for Central Europe, modified after [63].

3. Materials and Methods

3.1. Sampling

For the study, a total of 45 samples were collected from outcrops in the Tunjice Hills (Figure 1c). They belong to the mudstones according to the grain size classification of Udden–Wentworth and the marlstones and clay stones based on their CaCO₃ content. The first group of 16 samples were taken from the Early Miocene succession (Egerian and Eggenburgian stages—Central Paratethys/Aquitanian and Burdigalian stages—global time scale; Figure 2) and belong to the Govce formation (referred to in this paper as the Early Miocene samples). The second group of 17 samples were taken from the Middle Miocene succession (Badenian stage—Central Paratethys/Langhian stage—global time scale; Figure 2) and belong to the Laško formation (referred to from this point on as the Badenian samples). The third group of 12 samples were of Middle Miocene age succession (Sarmatian stage—Central Paratethys/Serravallian stage global time scale; Figure 2) and belong to the Dol formation (referred to from this point on as the Sarmatian samples). The Early Miocene and partly Badenian samples were collected in advance in the area of the sedimentological section (Figure 3a,b) of the Doblíč stream [56,64], while the other Badenian samples and all Sarmatian samples were collected in freshly exposed outcrops for the purpose of this study. Due to the widespread soil and vegetation, the samples were collected unevenly. Age determination was based on geological maps [48,51] and nannoplankton age determinations [56]. The exact locations of the samples are given in Table S1.

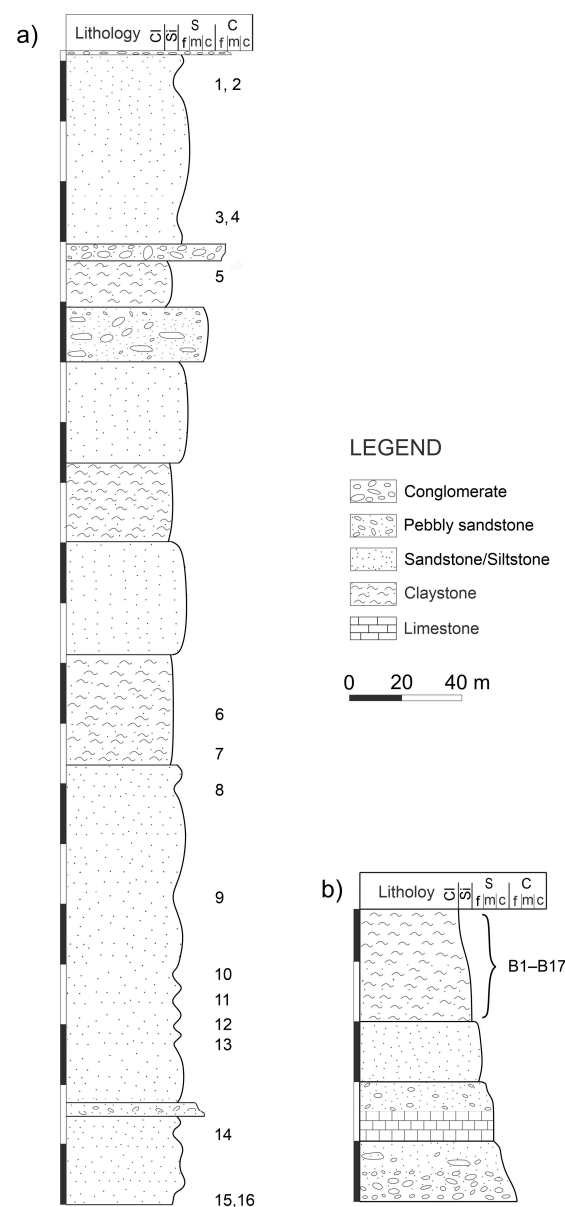


Figure 3. (a) Simplified Early Miocene sedimentary succession of the Tunjice Hills with sample locations E1–E16; (b) simplified significant sequence of the Badenian sedimentary successions. Samples B1–B17 were taken from the upper part of each sequence. Cl—claystone, Si—siltstone, S—sandstone, C—conglomerate, f—fine, m—medium, c—coarse.

3.2. Methods

3.2.1. Mineralogical Analysis

The samples were pulverized and homogenized to the fraction 5 to 10 μm by hand in an agate grinding mill and pressed into an aluminum holder. The mineral composition of the samples was measured by X-ray powder diffraction using a Philips PW3710 X-ray diffractometer with $\text{CuK}\alpha_1$ radiation and a secondary graphite monochromator. Data were collected at 40 kV with a current of 30 mA at a rate of $3.4^\circ 2\theta$ per minute over a range of 2 to $70^\circ (2\theta)$. Diffraction patterns were identified with X'Pert Highscore Plus 4.6 diffraction software using the PAN-ICSD database and the full-pattern fit method (Rietveld) for quantitative mineral phase analysis. Values below 0.1 wt.% are not detected.

3.2.2. Geochemical Analysis

Geochemical analysis was performed on all 45 samples, which were initially air-dried, crushed, and homogenized before final pulverization. Samples for whole-rock analyses of major oxides were performed by Activation Laboratories Ltd. (Ancaster, ON, Canada) and carried out by ICP-OES. Major element fusion was performed by a flux of lithium metaborate and lithium tetraborate and fused in an induction furnace. The molten melt is immediately poured into a solution of 5% nitric acid containing an internal standard and mixed continuously until completely dissolved. The samples are run for major oxides and selected trace elements (4B) on an ICP. Calibration is performed using 14 prepared USGS- and CANMET-certified reference materials. Standards used are: DNC-1, NOD-A-1, NOD-P-1, SY-4, and BIR-1a (see details in Table S2). Total organic carbon (TOC) was determined using the infrared LECO method. Carbon is measured as carbon dioxide in the IR cell as gases flow through the IR cells. The analysis is performed using ELTRA Instruments. Standards used were GS311-4, GS316-3, and GS317-5 (see details in Table S2). The determination of paleoweathering is based on the triangular plots of Nesbitt and Young [65] expressing the molar volumes of $[Al_2O_3/(Al_2O_3 + Na_2O + K_2O + CaO^*)]100$ (A-CN-K diagram) and the chemical index of alteration (CIA), where CaO^* represents the CaO content of the silicate minerals. The complete description of the calculation procedure can be found in detail in Bahlburg and Dobrzinski [5]. Provenance is determined using discriminant function diagrams by Roser and Korsch [66]. The diagrams divide the sedimentary rocks into four different provenances (quartzose sedimentary provenance, felsic, intermediate, and mafic igneous provenance) and are based on the major oxides and the ratio between the major oxides, based on calculations given in Oni et al. [67]. Tectonic settings based on Bhatia [68] tectonic discriminant functions are founded on the ratios of TiO_2 and $Fe_2O_3 + MgO$, and of Al_2O_3/SiO_2 and $Fe_2O_3 + MgO$ and of SiO_2 versus $\log(K_2O/Na_2O)$ after Roser and Korsch [66]. Tectonic settings are based on discrimination diagrams of Verma and Armstrong-Altrin [3] and differ according to low silica content ($>35\% - \leq 63\%$) and high silica content ($>63\% - \leq 95\%$). The discriminant function of Verma and Armstrong-Altrin [2] separates the active and passive margin settings. The entire procedure with the calculation formulas is described by [2] and the supplementary files therein.

4. Results

4.1. Mineralogy

The quantitative mineral composition of the samples is shown in Figure 4; the values can be found in Table S3. The quartz content of the Early Miocene samples varies up to 35.4 wt.%, albite up to 33.1 wt.% and calcite up to 45.4 wt.%. Dolomite ranged up to 24.4 wt.%, illite from 0.2 to 32.5 wt.%, muscovite from 0.3 to 15.6 wt.%, and montmorillonite from 0.2 to 29.6 wt.%. Kaolinite and pyrite content is low and varies up to 3.2 wt.% for kaolinite and up to 1.2 wt.% for pyrite. Cristobalite content varies up to 13.8 wt.%, but it is generally detected in lower amounts or not at all. The common content of clinocllore is up to 5.5 wt.%, but in one sample, its content is 54.2 wt.%.

The majority of Badenian sediments contain quartz in amounts ranging from 12.5 to 55.3 wt.%, calcite in amounts ranging from up to 62.5 wt.%, and dolomite in amounts ranging up to 44.4 wt.%. Muscovite content varies from 1.8 to 23.6 wt.% and clinocllore up to 13.4 wt.%. Clay minerals occur frequently. Albite content varies from 0.9 to 12.9 wt.%, illite up to 33.3 wt.%, montmorillonite up to 6.1 wt.%, and kaolinite up to 4.7 wt.%. Other minerals (cristobalite, tridymite, microcline, anorthite, pyrite, hematite) commonly occur in amounts lower than 2 wt.%.

The quartz content of the Sarmatian samples varies from 17.8 to 67.6 wt.%, calcite up to 28.6 wt.% and dolomite up to 46.4 wt.%. Muscovite content varies from 2.6 to 26.7 wt.%, clinocllore up to 9.1 wt.%, and albite from 1.4 to 9.7 wt.%. Clay minerals are common. Illite content varies between 0.8 and 19.2 wt.%, kaolinite content between 0.6 and 7.5 wt.%, and montmorillonite content up to 21.2 wt.%. Other minerals (tridymite, microcline, anorthite, pyrite, hematite) occur rarely and generally in amounts below 1 wt.%.

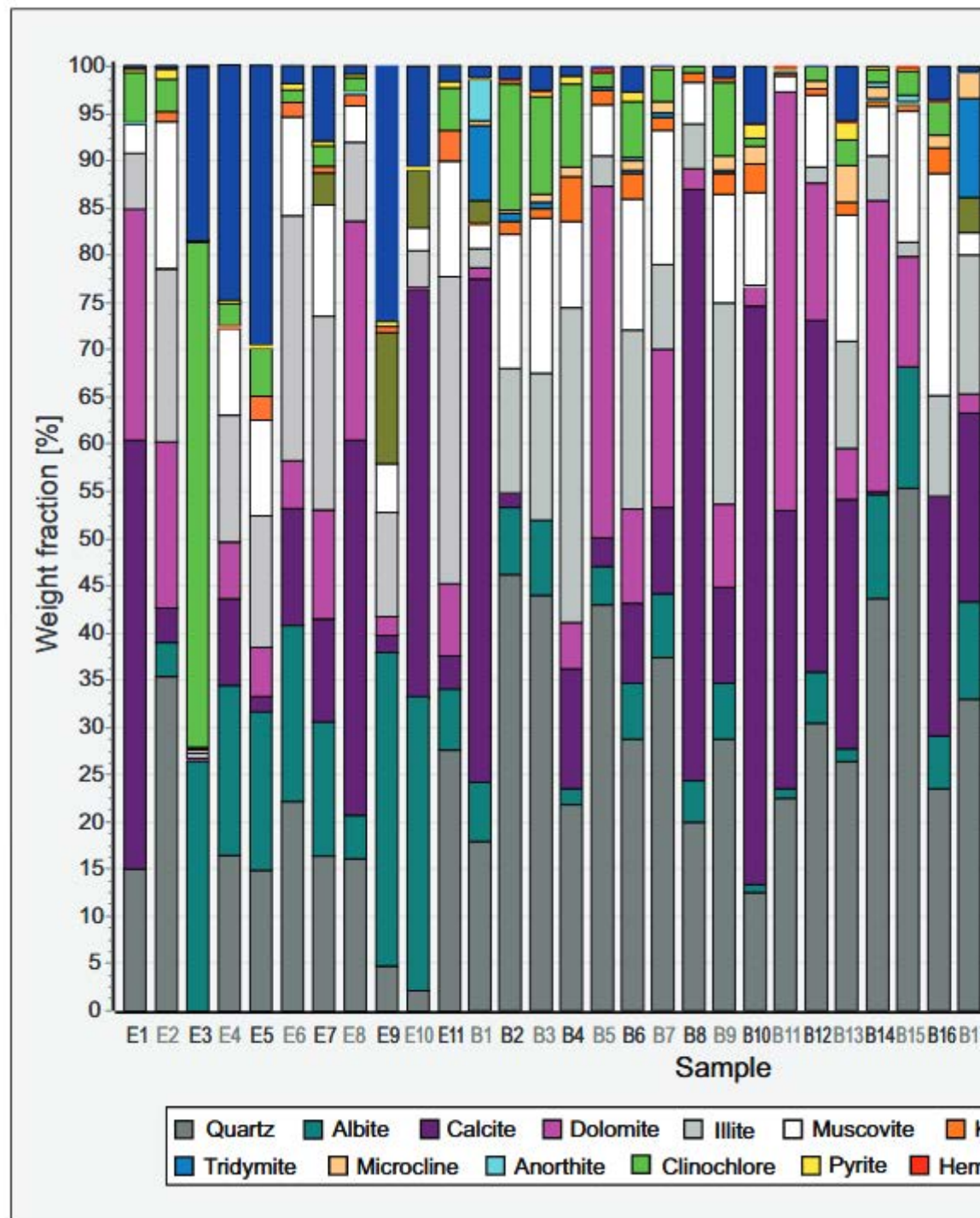


Figure 4. Quantitative mineral composition of samples in wt (%) in Tunjice Hills.

The XRD patterns show the presence of large amounts of quartz in all samples and a slightly lower, but still very abundant, occurrence of calcite, muscovite, and albite. The weight ratio of quartz and calcite is often inversely proportional, but in some cases, their weight ratio is very similar, for example, in sample B13, where their weight ratio is almost equal. Significantly less calcite and dolomite and higher amounts of quartz, montmorillonite, kaolinite, and anorthite are determined in the Sarmatian samples than in the Badenian samples. Cristobalite is detected only in the Early Miocene samples. The amounts of other minerals in the Badenian and Sarmatian samples (see Figure 4) are similar.

Significant differences can be observed in the amount of quartz and albite, which is lowest in the samples from the early Miocene. There is a significant difference in sample E3, in which no quartz and calcite were detected and in which clinocllore is abundant, and in sample E1, in which no albite was detected. The highest quartz values are found in the samples from the Sarmatian. There is generally very little calcite and dolomite in some samples from the Sarmatian, while montmorillonite is only present in a few samples from the early Miocene and the Sarmatian. The proportion of kaolinite, pyrite, muscovite, calcite and dolomite varies from sample to sample and the value is not tied to a specific group of samples.

4.2. Geochemistry Composition (Major Oxides)

The content of each major oxide varies considerably among the main groups of samples (Early Miocene, Badenian, Sarmatian) and within each group (Table S4). The silica content is inversely proportional to the CaO content (Figure 5). The lowest silica content is found in the Early Miocene samples (from 24.41% to 57.47%), while the alumina content varies from 1.39% to 15.67% and the CaO content from 3.33% to 36.11% (Figure 5). Fe₂O₃ content varies from 0.94% to 5.79%, MgO content from 0.51% to 5.04%, and Na oxides from 0.06% to 0.55%, and K oxides from 0.19% to 2.93%. The silica content in Badenian samples varies from 20.18% to 71.46%, CaO from 0.67% to 34.84%, and alumina from 4.63% to 13.49%. Fe₂O₃ content varies from 1.09% to 4.84%, MgO from 1.27% to 8.1%, Na oxides from 0.44% to 2.38%, and K oxides from 0.44% to 2.38%. The youngest samples (those from the Sarmatian) range from 44.26% to 82.75% in silica content, in CaO content from 0.09% to 15.96%, and in alumina content from 4.55% to 13.43%. Fe oxides content in the samples varies from 1.37% to 6.24%, Mg oxides from 0.45% to 4.76%, Na oxides from 0.13% to 0.91%, and K oxides from 0.85% to 2.78%. Mn, Ti, and P oxides are represented with less than 1% in all samples.

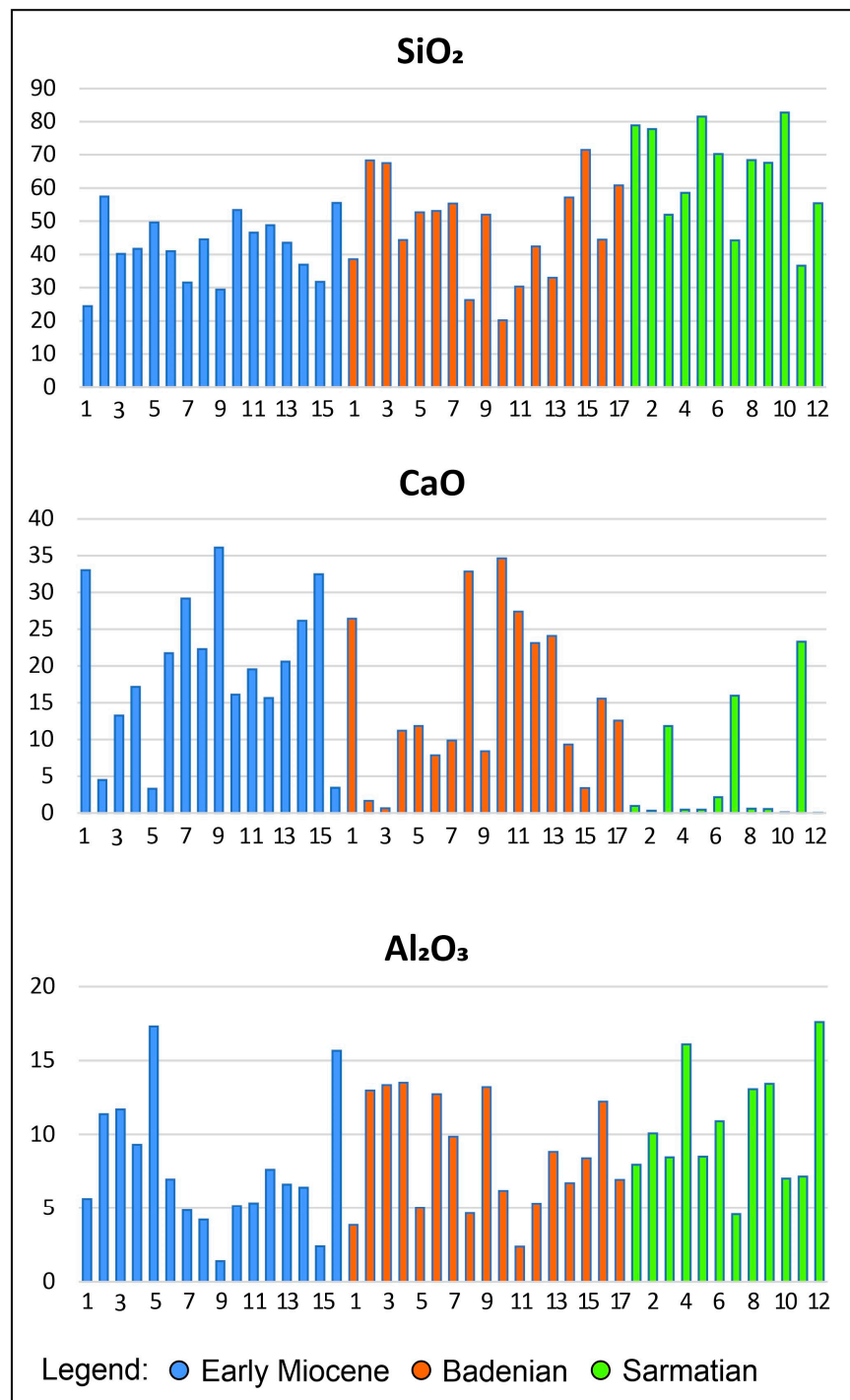


Figure 5. Content of SiO₂, CaO and Al₂O₃ in individual samples.

Based on the chemical classification diagram of Herron [69], the mudstones are classified mainly as shales, wackes, and litharenites (Figure 6).

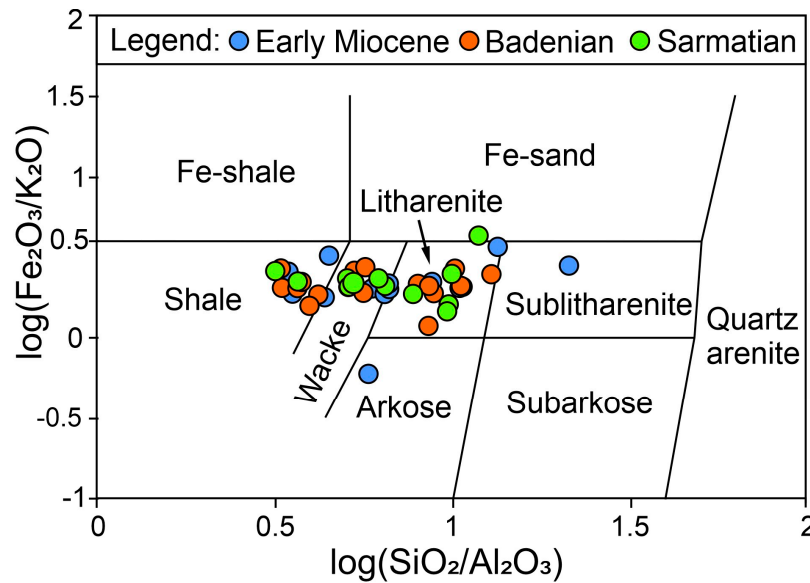


Figure 6. Geochemical classification of the Tunjice Hills sedimentary rocks using $\log(\text{SiO}_2/\text{Al}_2\text{O}_3)$ versus $\log(\text{Fe}_2\text{O}_3/\text{K}_2\text{O})$, after Herron [69].

4.3. Ternary and Discriminant Diagrams Based on Major Oxides

The samples from the Tunjice Hills are arranged on the left side of the A-CN-K triangular plot and show a linear trend subparallel to the A-CN junction (Figure 7). The Sarmatian samples have the highest average of Al_2O_3 content, while the Early Miocene samples have the lowest average of Al_2O_3 content. The samples were uniformly distributed subparallel to the A-CN joint. The diagram shows the greatest agreement with the weathering trends of tonalite and granodiorite. The average CIA (chemical index of alteration) value is 53.55 for the Early Miocene samples, 60.08 for the Badenian samples, and 78.03 for the Sarmatian samples. The lowest and highest CIA values come from the Early Miocene samples, with 13.6 being the lowest and 94.8 the highest.

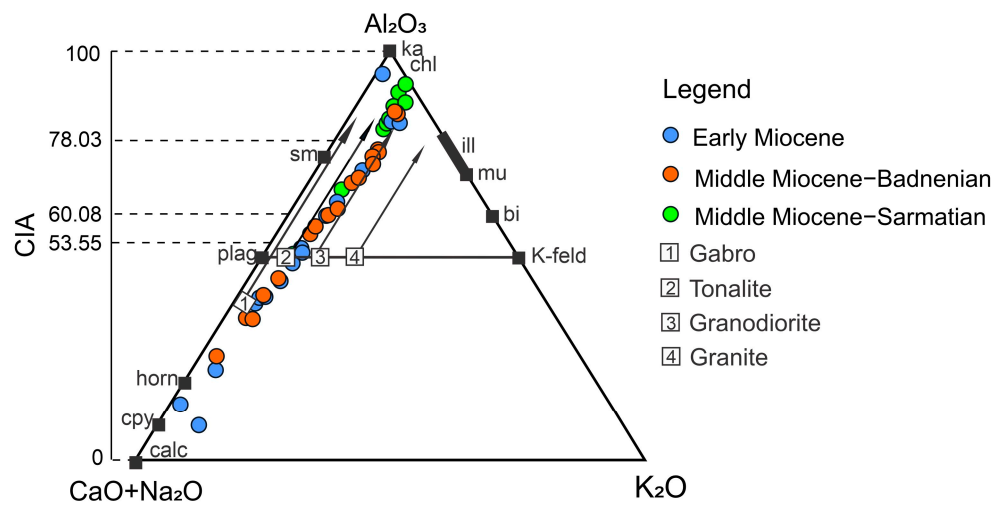


Figure 7. Molecular proportions of the A-CN-K ternary diagram [65] for the sedimentary rocks in the Tunjice Hills.

According to the discriminant function diagrams of Roser and Korsch [66], the majority of the Early Miocene samples in the first diagram (Figure 8a) can be assigned to the intermediate field, two samples to the recycled, and one to the mafic field. In the second diagram (Figure 8b), the majority of the samples plot into the recycled field—one to the mafic field and one to the felsic one. The samples that plot into the mafic field are not identical in both diagrams. The Badenian samples are in the recycled and intermediate provenance fields in both diagrams, but in the second diagram (Figure 8b), many samples lie on the border between intermediate and recycled fields. Most of the Sarmatian samples fall into the recycled field in the first diagram and in the second diagram (Figure 8b), similar to the Badenian samples, into the boundary between intermediate and recycled provenance. Two samples from the Sarmatian fall into the mafic field. While the first diagram shows a tendency to assign the younger sediments to the recycled field and the older ones to the intermediate field (Figure 8a), the samples in the second diagram (Figure 8b) show no characteristic contribution.

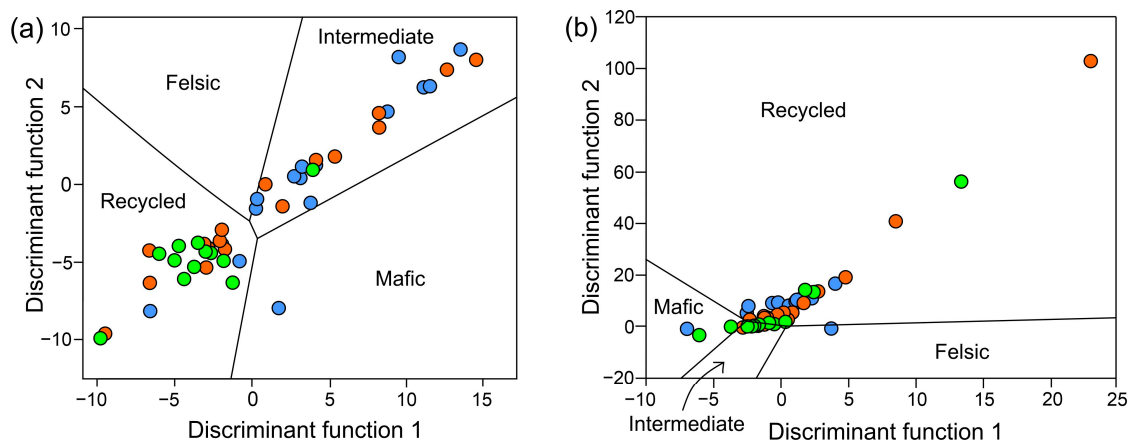


Figure 8. Discrimination diagrams for the provenance signature of the Tunjice Hills sedimentary rocks using major oxides (a) and the ratios between major oxides (b) after Roser and Korsch [66]. The legend of the samples is shown in Figure 7.

The $\text{Al}_2\text{O}_3/\text{TiO}_2$ ratio of the Early Miocene samples is 28.19. The Early Miocene samples contain two samples with ratios greater than 80, which increases the ratio. Excluding these two samples, the $\text{Al}_2\text{O}_3/\text{TiO}_2$ ratio is 21.79. The ratio of the Badenian samples is 18.26 and 16.41 for the Sarmatian samples.

The majority of Early Miocene and Badenian samples in the discriminant diagram of SiO_2 versus $\log(\text{K}_2\text{O}/\text{Na}_2\text{O})$ after Roser and Korsch [66] plot into the oceanic island arc setting, and the majority of Sarmatian samples plot into the field of active continental margin setting (Figure 9).

Based on Bhatia's [68] tectonic discriminant function of major elements, all three sample groups are unevenly distributed, and based on the ratio of TiO_2 and $\text{Fe}_2\text{O}_3 + \text{MgO}$ (Figure 10a), are predominantly placed in the active continental margin and continental island arc region. Based on the ratio of $\text{Al}_2\text{O}_3/\text{SiO}_2$ and $\text{Fe}_2\text{O}_3 + \text{MgO}$, most samples plot in the field of the continental island arc and the active continental margin field (Figure 10b). Individual samples lie within the oceanic island arc and passive margin. The majority of samples in both diagrams plot outside of any field (Figure 10a,b).

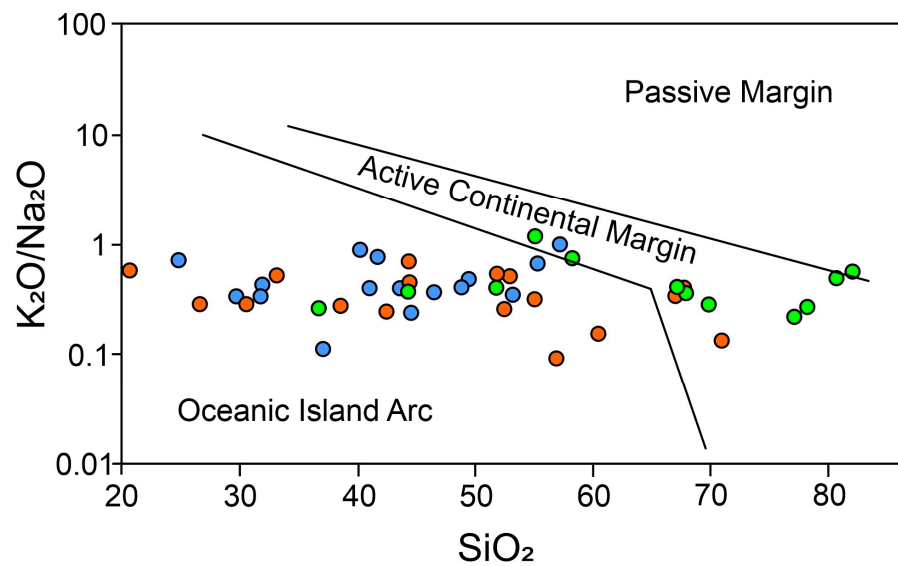


Figure 9. Tectonic setting discriminant plot after Roser and Korsch [66]. Samples from the Tunjice Hills plot into the oceanic island arc and active continental margin fields. The legend of the samples is shown in Figure 7.

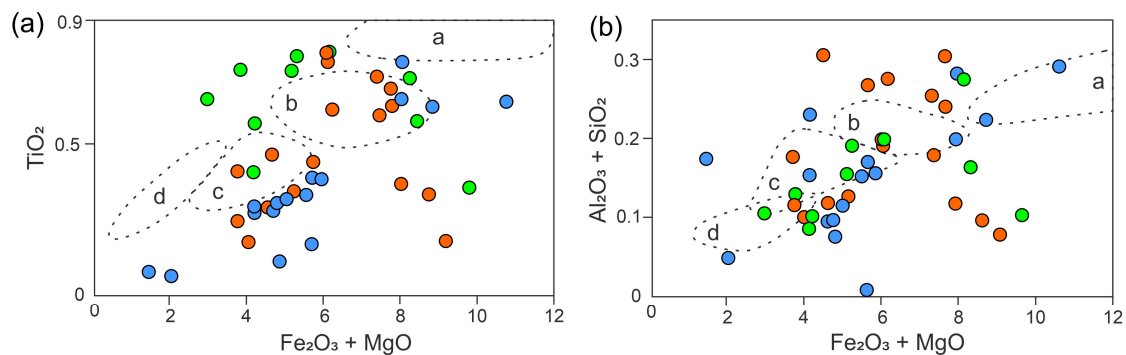


Figure 10. (a) Bivariate plot of TiO_2 versus $\text{Fe}_2\text{O}_3 + \text{MgO}$ diagram for the Tunjice Hills sedimentary rocks after Bhatia [68]. (b) Bivariate plot of $\text{Al}_2\text{O}_3/\text{SiO}_2$ and $\text{Fe}_2\text{O}_3 + \text{MgO}$ diagrams for the Tunjice Hills sedimentary rocks after Bhatia, [68]; a—oceanic island arc, b—continental island arc, c—active continental margin, d—passive margin. The legend of the samples is shown in Figure 7.

Slightly different results in determining the tectonic setting are provided by the low- and high-silica diagrams of Verma and Armstrong-Altrin [3]. In the low-silica diagram (Figure 11a), most of the Early Miocene samples are assigned to the collision and rift zone, and only one sample plot into the arc field. The majority of the Badenian samples and all of the Sarmatian samples are assigned to the collisional field. In the high-silica diagram (Figure 11b), all Early Miocene and Badenian samples and the majority of Sarmatian samples are in the collisional field. Only two samples from the Sarmatian fall within the rift field.

According to the Verma and Armstrong-Altrin [2] discriminant function (Figure 12), all Badenian and Sarmatian samples and the majority of Early Miocene samples are in the passive margin setting, and only two Early Miocene samples are in the active margin setting. A single sample (the same as in the low-silica diagram) is plotted in the arc field.

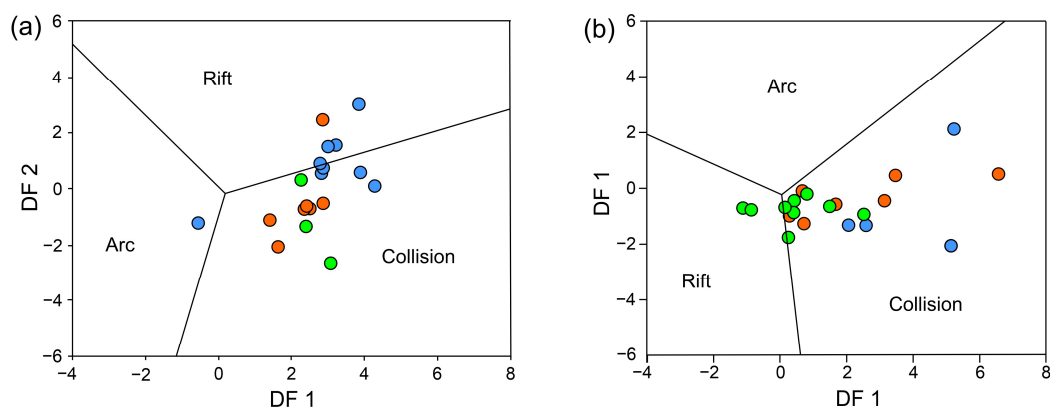


Figure 11. Multidimensional diagrams after Verma and Armstrong-Altrin [3]. (a) Samples from the Tunjice Hills are plotted in the collision (high-silica) field. (b) Samples from the Tunjice Hills are plotted in the collision and rift (low-silica) field. The legend for the samples is shown in Figure 7.

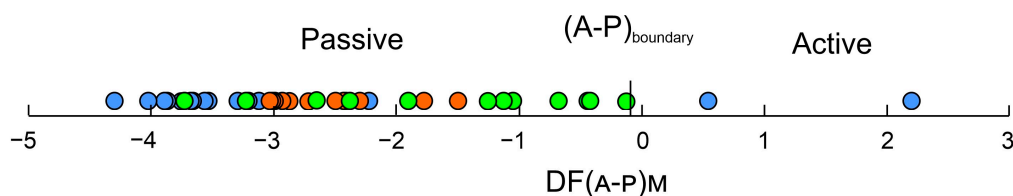


Figure 12. Discriminant function after Verma and Armstrong-Altrin [2]. The majority of the samples from the Tunjice Hills are plotted in the passive margin field. The legend of the samples is shown in Figure 7.

5. Discussion

5.1. Paleoweathering

According to the ternary diagram of molecular proportions (Figure 7), the samples are arranged on the left side, with the weathering trend subparallel to the A-CN side. This characterizes the initial weathering trends of igneous rocks with trends in the removal rates of Na and Ca from plagioclase [65] and also suggests that the weathering process had a greater influence on rock composition than diagenesis and metamorphism [70]. The Sarmatian samples have the highest CIA value (78), and the Early Miocene samples have the lowest CIA value (53.55). Some Early Miocene and Badenian samples have very low CIA values (below 50). In contrast, two samples show strong weathering with CIA above 90. The ACNK diagram, in our case, most clearly shows the tendency for older samples to be less susceptible to chemical weathering, while the younger samples were more susceptible. Considering that all samples are fine-grained and geochemically belong to shale, litharenite, and wacke (Figure 6), the possibility of ordering the samples by grain size is minimized.

CIA values of about 50 are considered unweathered, and CIA near 60 indicates weak weathering [70]. CIA values between 60 and 80 indicate moderate chemical weathering [71]. Values above 80 indicate extreme chemical weathering [71]. The reason for the rather high value (78) of CIA in the Sarmatian samples is most likely to be the prevailing warm and humid weathering conditions [5], while low-to-moderate weathering (53–60) reflects cold and/or arid climatic conditions in the source area [11]. Alternating warmer and cooler temperatures in the study area coincides well with global and regional temperature changes [41,63,72].

The mineral composition does not indicate any significant paleoweathering trend within the sample groups, as is in the case for the geochemical composition. Clay minerals are the remains of feldspars and are the most common products of chemical weathering. The significant difference is the proportion of albite, which is higher in the Lower Miocene sediments. Its quantity has no influence on the amount of clay minerals, which are com-

parable to the amount of the Badenian and Sarmatian samples. Montmorillonite belongs to the smectite group and is formed during the weathering of volcanic ash. Its occurrence in samples from the Early Miocene can be correlated with the weathering of volcanic rock from the Oligocene. Illite clays are the main component of ancient mudstones and shales. Kaolinite is less common than illite, which may be due to the higher salinity of the water. Chlorite and illite originate from less weathered intrusive and metamorphic rocks. Chlorite, on the other hand, is not resistant to chemical weathering and is an important detrital component in areas with low chemical weathering. These areas are characterized by colder climates [73]. The climate in the Central Paratethys changed significantly between the Early and Middle Miocene [24,74]. While the Egerian and Eggenburgian flora indicate a warm and humid climate in the western part of the Central Paratethys [24,73,75], the flora in the Karpatian and the Ottnangian indicate milder temperatures [76]. In fact, even arid climatic conditions are present locally in the Early Miocene [77]. This coincides with the Middle Miocene Climatic Optimum (MMCO), when, due to low global ice volume, the temperature of seawater rose slightly [63] and caused an expansion of bioproduction and biodiversity [24,61]. During the Badenian, stable subtropical conditions prevailed in the Central Paratethys [78]. Carbonate sequences in the Central Paratethys reflect warmer, subtropical conditions in the Sarmatian [74], which is also confirmed by a negative peak in the oxygen isotope curve [79].

It appears that despite the relatively similar sedimentary rocks, tectonic units or geological time, the trend of paleoweathering is very specific and limited only to the narrow local area [14,15,25,80,81].

5.2. Provenance

5.2.1. Mineralogical Approach

Quartz occurs in most sedimentary, metamorphic, and igneous rocks [82]. As a detrital component, it is highly resistant to physical and chemical weathering, so it is usually preserved in large quantities and is the most abundant terrigenous mineral in sandstones [83,84]. In the case of the Tunjice Hills, different types of quartz are present. Detrital quartz in the form of monocrystalline or polycrystalline quartz grains and metamorphic and igneous quartz are found in the sandstones [56]. The sandstones of the Tunjice Hills also contain considerable amounts of authigenic quartz, formed by authigenic processes during the cementation of sands [56]. Quartz is a common mineral in various hinterland types and can be found in volcanic rocks (tonalite, granodiorite) and metamorphic rocks (inclusions in eclogites, garnet, omphacite, and kyanite); therefore, its origin could be related to the provenance from the Austroalpine units, from the Eisenkappel magmatic zone [51,54,85,86] or the Smrekovec volcanic complex [54].

Carbonate minerals occur in almost all sedimentary rocks. The most common and most stable polymorph of calcium carbonate mineral is calcite [87]. Calcite determined in the studied samples is most likely of authigenic origin as calcite cement, formed in shallow marine environments [56,88]. Additionally, detrital calcite and dolomite minerals may be associated with grains from carbonate rocks of the Southern Alps. During the Miocene, the transgressions of the Central Paratethys flooded the wider area several times [44,60,78,88], which led to larger amounts of mainly calcite—also aragonite and dolomite—which is excreted biogenically by marine organisms (skeletons, shells) [47]. The Sarmatian samples contain less calcite and dolomite compared to the Badenian samples from the Tunjice Hills, which could be attributed to variations in seawater salinity. Salinity began to decrease in the Sarmatian [44,74], which most likely led to a decrease in calcite in the early Sarmatian samples. Generally, the late Sarmatian is characterized by increased carbonate content [89]; however, the sedimentation in the Tunjice Hills most likely ended before that. Differences in the amounts of dolomite and calcite may also indicate differences in the transport system during the Badenian and Sarmatian. The presence of dolomite may be related to terrigenous origin. Its presence in the form of dolomite cement is unlikely [56]. Dolomites may be

associated with the influx of material [88] from the Southern Alps, where Triassic dolomites occur. This suggests a local origin and a provenance from the north.

Feldspars pose a challenge for accurate source rock identification because they are ubiquitous in metamorphic and igneous rocks [90] and are chemically and mechanically unstable in the sedimentary environment [83]. In the Tunjice Hills, feldspars are represented by plagioclase (Ca and Na feldspars) and alkali feldspars. Their origin could be related to the low-grade metamorphic rocks of Mt. Kranjska Reber and/or to the Smrekovec volcanic complex [54,91]. The possible hinterland of the feldspars might also represent the Periadriatic magmatic zone or the Austroalpine units of the Eastern Alps [85,88,92].

Chlorites are commonly found in metamorphic rocks, particularly greenschists and chlorite shales, as well as altered igneous rocks [83]. Clinocllore (Mg-chlorite) has been detected in Badenian and Sarmatian samples from the Tunjice Hills. Mg-rich chlorite is typically found in evaporite deposits. Furthermore, chlorite forms during burial diagenesis and metamorphism [73]. Thick evaporite sediments were deposited in the Transcarpathian Basin, Transylvanian Basin, and Carpathian Foredeep (PBS) during the middle Badenian [78,93,94], which can be attributed to a salinity crisis. Evaporite sediments were not detected in the Tunjice Hills nor in the SW Central Paratethys [37], but their remains may have been washed away. The origin of the clinocllore in Badenian and Sarmatian rocks is likely associated with detrital material from the metamorphic rocks of the Eastern Alps and volcanic rocks of the Smrekovec area, as there is no objective difference in their amounts. It is unlikely that they originated from evaporite deposits.

Illite and muscovite are frequently present in similar quantities in the samples of the Tunjice Hills. Generally, illite has its origin in micas, usually muscovite, and forms through chemical alterations or in metamorphic or peri-magmatic conditions [95]. Muscovite and illite in the samples from the Tunjice Hills are most likely associated with metamorphic and magmatic origin in the Austroalpine units and the Smrekovec area.

Pyrite is a common mineral in various rock types. Pyrite formation is more abundant in marine environments than in non-marine ones because of the dissolution of sulfate and iron minerals due to organic matter [96]. The presence of pyrite in the studied samples is related to establishment of marine environments as a consequence of the Early and Middle Miocene transgression of the Central Paratethys [24,44,97]. This resulted in the precipitation of pyrite and other related minerals, such as glauconite [56].

5.2.2. Geochemical Approach

The presence of major elements and their ratios can provide reliable information about the origin of the source area [98–100]. Of the major elements, Al_2O_3 and TiO_2 are considered immobile during weathering, transport, and diagenesis, so their ratio is used to infer source rock composition [9,101–103]. Their ratio in the Early Miocene samples is 28.19 and corresponds to a felsic igneous source cf. [104]. The ratio in the Badenian samples is 18.26 and 16.41 in the Sarmatian samples. Both correspond to an intermediate source (values for granitic, igneous, and sedimentary rocks).

The discriminant diagram of Roser and Korsch [66] separates four major source areas. Samples from the Tunjice Hills plot mostly into the recycled and intermediate fields in diagram A (Figure 8a) and are at the boundary between the recycled and intermediate fields in diagram B (Figure 8b). The differences in provenance according to the diagram by Roser and Korsch [66] (Figure 8a) between the Early Miocene and Sarmatian samples of studied rocks are clearly evident.

Samples that plot into the intermediate igneous provenance field have lower silica content (below 50%). This suggests a higher amount of alumina and CaO [105], and their origin may be associated with parts of the Eastern Alps. Quartzose sedimentary provenance indicated that the sediments were subjected to recycling. Furthermore, the source material was predominantly quartz-rich sedimentary rocks, and to a lesser extent igneous rocks. The rocks are rich in silica and poor in alumina, and the CaO content is low.

The origin from the recycled orogen fits well with the origin of the sediments in the collision zone, which corresponds to the origin from the Alps. The active Europe convergence throughout the Oligocene and Miocene [106] could lead to the sediments originating from the uplifted Dinaric and Southern Alpine blocks such that most of the sediments could be derived from the locally uplifted blocks of the Southern Alps [38,107] to the north and the Dinarides to the south of the Tunjice Hills. Considering that the Central Paratethys covered the area south of the Tunjice Hills in the Early and Middle Miocene [38] and that the lowlands with Quaternary sediments to the east still exist [88,108], the origin from the eastern side is minimal. Lowlands to the west enabled a marine gateway through the so-called Trans-Tethyan Corridor during the Karpatian and the Badenian [38,44,109,110]. The intermediate origin points at the sediments originating from the Alps, more precisely from the Karawanks [111,112], the Eastern Alps [85] or Triassic igneous rocks [113].

Since the A-CN-K diagram (Figure 4) shows the weathering tendency of granodiorite and subordinately of tonalite (majority of Badenian samples only), it is possible to conclude that the provenance of the sediments is also in the northeast, from the Eisenkappel magmatic zone [114].

5.3. Tectonic Setting

As demonstrated, the use of several different diagrams to determine tectonic setting turned out to be expedient. Six discriminant functions resulted in three different tectonic settings, which is difficult to justify despite the complexity of the area in the given environment at the transition between the Adriatic and European tectonic plates [45].

The multidimensional diagram based on the major oxides for low- and high-silica content, according to Verma and Armstrong-Altrin [3] and the discriminant function based on the major oxides, according to Verma and Armstrong-Altrin [2], gave rather unequal results. The majority of the samples fall within the collision field in the low- and high-silica diagram, and only a few samples plot into the rift field (Figure 11). In contrast, the samples in the discriminant function were plotted into the field of the passive margin (Figure 9). Such contradictory results were found in previous studies [15] in the western part of the PBS and Central Paratethys.

This disunity coincides well with abovementioned tectonic processes that continued from the Oligocene and were active during the Miocene [20]. Discriminant functions (Figure 11) indicate a strong dominance of the collision field, which indicates the tectonic setting in which the sediments were deposited in the basin. A distinct collision zone can therefore be traced in the samples of Badenian and Sarmatian age, while the activity of the major faults (Periadriatic and Sava Faults) can be detected throughout the whole period.

The discriminant function (Figure 12) shows a significant impact of the passive margin, indicating a strong prevalence of extension processes. Unexpectedly, these stem from the Lower Miocene onward. Since the formation of the PBS started in the late Early Miocene (as discussed earlier in this chapter), it was expected that the diagram would show the difference between the samples from the Govce formation and the other samples. It is difficult to explain the subjection of the sediments to a specific tectonic setting that did not yet exist at the time of sedimentation. However, the above findings stress that the discriminant function after Verma and Armstrong Altrin [3] shows the tectonic setting of the source rocks, while the discriminant function after Verma and Armstrong Altrin [2] shows the tectonic setting during sedimentation; nonetheless, caution in interpreting the results is advised.

The discriminant function after Roser and Korsch [66] (Figure 9) reveals another tectonic setting. It indicates that the majority of the Early Miocene and early Middle Miocene sediments were subjected to the oceanic island arc and the majority of the Sarmatian samples to the active continental margin. The study area is located at the triple junction of the Alpine orogen, the Pannonian Basin System and Dinaric tectonic units [45] and the oceanic island arc setting is not expected in this area [22,115,116]. However, it is more likely that the diagram reflects the tectonic setting of the source rocks from the Eastern and Southern

Alps. These rocks were transported to the study area in the Neogene with different transport processes. Oceanic and more frequently continental island arcs have been defined in the Karawanks [34], and constitute the Late Paleozoic–Mesozoic geodynamic evolution in the Tethys area [117–119]. These differences between the results of the Badenian and Sarmatian samples could be related to paleogeographic changes that allowed a different sedimentary input.

Bhatia's [68] diagrams proved to be very unreliable in this study because most of the samples plot outside of any field (Figure 10). The reason for this could be the influence of chemical weathering on the sediments. Therefore, an additional investigation was carried out, excluding all samples with CIA above 80 (Figure 13a,c). The investigation helped ascertain that these samples fell out of the margins of the diagram (Figure 13a), but not in the case of the ratio of Fe and Mg oxides to Al and Si oxides (Figure 13c). In addition, another inquiry was conducted excluding samples whose CIA was less than 30. In the diagram (Figure 13b), the results show that the samples are less scattered, but in the case of Fe and Mg oxides versus Al and Si oxides (Figure 13d), there is no obvious difference. It bears emphasizing that chemical weathering does not play a significant role in the tectonic discrimination functions. However, some Badenian samples from the Tunjice Hills fall within the range of the continental island arc field (Figures 10a and 13a,b). This may be related to active intra-plate calc-alkaline volcanism in the Middle Hungarian Zone. Various processes, such as mantle plumes of hot rock from the Earth's mantle or thinning of the lithosphere resulting in the melting of the mantle [120], may also affect sedimentation in the western part of the PBS. The inaccuracy of these diagrams has already been discussed [121]; therefore, great caution should be exercised when using and relying solely on these discriminant diagrams. However, the diagrams were found to be a good indicator for determining the source material in the southwestern part of the PBS [25].

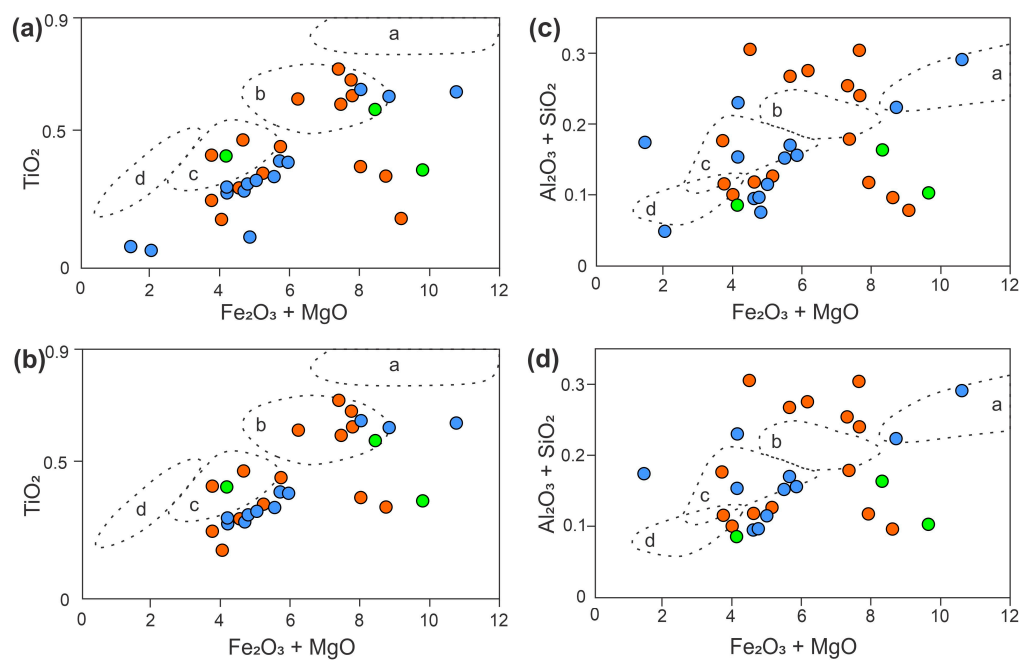


Figure 13. (a,b) Bivariate plot of TiO_2 versus $\text{Fe}_2\text{O}_3 + \text{MgO}$ diagram for the Tunjice Hills sedimentary rocks after Bhatia [68]; (c,d) bivariate plot of $\text{Al}_2\text{O}_3/\text{SiO}_2$ and $\text{Fe}_2\text{O}_3 + \text{MgO}$ diagrams for the Tunjice Hills sedimentary rocks after Bhatia [68]; (a,c) diagrams exclude samples with CIA > 80; (b,d) diagrams exclude samples with CIA > 80 and CIA < 30. The legend of the samples is shown in Figure 7. Explanatory notes: a—oceanic island arc, b—continental island arc, c—active continental margin, d—passive margin.

Interpretation of Tectonic Setting of the Tunjice Hills (Western Central Paratethys)

Various tectonic processes influenced the development of the studied area from the Miocene onwards, starting with the collision of the Adriatic and European lithospheric plates [20,35,36]. Considering that the Tunjice Hills are located at the western margin of the PBS at the conjunction of the Alps and the Dinarides, it can be emphasized that the results suggest that both rifting and collision played an important role in sedimentation in the Tunjice Hills during the Early and Middle Miocene. The basement of the PBS consists of ALCAPA (Alpine–Carpathian–Pannonian) and Tisza–Dacia mega-units and a Dinaridic tectonic unit [18,29,34]. The movement of the Adriatic–European plate, which triggered the Alpine collision, caused the activity of several faults, folds, and overthrusts in the area of the junction between the Alps and the Dinarides [122]. The collision caused pronounced changes: dextral movement of the Padiadriatic Fault (PAF) over 100 km during the Miocene [107,123,124], the thrusting of the External Dinarides, which is estimated to be post-Eocene and Early Miocene in age [125,126], and the activation of the Sava fault, resulting in the folding of the Late to Middle Miocene strata [106]. According to recent studies [127], these faults are still active. The collision was one of the reasons for subduction, subsidence and extension of the lithosphere that led to the evolution of the back-arc type PBS in the late Early Miocene. Extension led to the thinning of the crust and subsidence and formation of a back arc-type basin [32,61,128–132]. The influence of the passive margin, connected with the formation of the PBS and the impact of arc setting were not expected in the Early Miocene sedimentation in the Tunjice Hills. The explanation of the arc setting is not certain. It is possible that volcanic activity in the Oligocene (Smrekovec complex) influenced sedimentation at the beginning of the Early Miocene. However, sedimentation in the Middle Miocene may be related to volcanic activity in intra-plate settings near the Middle Hungarian Zone. These processes significantly influenced the sediments and sedimentation in the PBS and its margins [15,38,78,124] that in our case can be traced in the discriminant function (Figure 12). According to the sequence of the events and processes described, it can be emphasized that Early Miocene sedimentation was more influenced by the collision, and in the Middle Miocene, sedimentation was more influenced by rifting.

6. Conclusions

Sedimentation in the Tunjice Hills was subjected to pronounced tectonic, climatic, and provenance changes in the Early and Middle Miocene that were defined by geochemical and mineralogical analyses. From the data presented, geochemical and mineralogical analyses allowed for the conclusion that detailed fingerprints of provenance and tectonic settings may be traced in sediments from the different tectonic backgrounds and regions. In the case of the relatively well-known Alpine–Pannonian region, the use of various geochemical functions gave a unique insight into the purpose of each function.

- The heterogeneous mineral and chemical composition and alteration in their abundance suggest a markedly wide area of origin of the sediments. The studied rocks are rich in quartz and poor in feldspars and indicate quartzose sedimentary provenance. Source areas of sediments were connected with an origin from the Southern Alps, Austroalpine units of the Eastern Alps, Eisenkappel magmatic zone, and the Smrekovec volcanic complex.
- The paleoweathering ternary diagram turned out to be very reliable. The Early Miocene rocks of the Tunjice Hills have the lowest CIA, while the youngest rocks (Badenian and Sarmatian) have the highest CIA value. Results are consistent with the differences in paleoclimatic conditions during the Early and Middle Miocene, which ranged from colder to warmer and more humid climates. The latter corresponds well with the MMCO.
- The discriminant function of Roser and Korsch [66] and the discriminant function of Verma and Armstrong Altrin [3] have proved to be very useful in determining the tectonic setting of the source sediment. It appears that the source sediments in the Tunjice Hills were subjected to oceanic island arc and collision setting, which

corresponds well with the hinterland. However, the passive margin connected to the evolution of the Pannonian Basin and the possible influence of the intra-plate settings near the Middle Hungarian Zone was also identified.

- The discriminant functions of Bathia [68] are the only ones that were unreliable. Additional analyses showed that the diagram did not include the samples in the specific groups and the results could not be put into context, so the use of the diagram is not recommended.
- Sedimentation in the Tunjice Hills, located south of the Southern Alps and representing the western margin of the PBS, was strongly influenced by both active and passive margin settings. This was demonstrated by multidimensional diagrams, as presented by Verma and Armstrong Altrin [2,3]. However, the results did not allow for the determination of the specific influence of each setting during a given period. Based on the regional tectonic evolution of the PBS and Alpine orogen, it is important to note that the collision zone had a stronger impact on sedimentation during the Early Miocene and the rift setting during the Middle Miocene. Nevertheless, the sedimentary input may have originated from a collision zone and had been deposited in an area where the rift zone was already active.

Supplementary Materials: The following supporting information can be downloaded at <https://www.mdpi.com/article/10.3390/app14020537/s1>. Table S1: Locations of the samples using the WGS84 coordinate system, and their respective ages. Table S2: Processes for the separate geochemical analysis used in the study. Table S3: Quantitative mineral composition of the Early Miocene (E1–E11), Badenian (B1–B17), and Sarmatian (S1–S12) samples of the Tunjice Hills. Table S4: Major oxides, LOI, TOT/C, and CO₂ abundance (%) in samples from the Tunjice Hills.

Author Contributions: Conceptualization, K.I., R.B. and M.V.; methodology and formal analysis, K.I. and M.V.; investigation, K.I., R.B. and M.V.; writing—original draft; K.I.; writing—reviewing and editing, K.I., R.B. and M.V., visualization, K.I.; project administration, K.I.; funding acquisition, K.I. and R.B. All authors have read and agreed to the published version of the manuscript.

Funding: The research was funded by the IAS Postdoctoral Research Grant Scheme, to which we express our deep gratitude. In addition, the authors gratefully acknowledge financial support from the Slovenian Research and Innovation Agency (Research Core Funding P1-0025—“Mineral Resources”).

Institutional Review Board Statement: Not applicable.

Informed Consent Statement: Not applicable.

Data Availability Statement: The authors confirm that the data supporting the findings of this study are available within the article and its supplementary materials.

Acknowledgments: Many thanks to Miha Marinšek for the ostracod analyses he used to confirm the age of some Sarmatian samples.

Conflicts of Interest: The authors declare no conflicts of interest.

Abbreviations

The following abbreviation is used in this manuscript:

PBS	Pannonian Basin System
CIA	Chemical index of alteration
TOC	Total organic carbon
MMCO	Middle Miocene Climatic Optimum

References

1. Zakir, H.M. Major, Trace, and REE Geochemistry of the Meghna River Sediments, Bangladesh: Constraints on Weathering and Provenance. *Geol. J.* **2020**, *55*, 3321–3343. [[CrossRef](#)]
2. Verma, S.P.; Armstrong-Altrin, J.S. Geochemical Discrimination of Siliciclastic Sediments from Active and Passive Margin Settings. *Sediment. Geol.* **2016**, *332*, 1–12. [[CrossRef](#)]

3. Verma, S.P.; Armstrong-Altrin, J.S. New Multi-Dimensional Diagrams for Tectonic Discrimination of Siliciclastic Sediments and Their Application to Precambrian Basins. *Chem. Geol.* **2013**, *355*, 117–133. [[CrossRef](#)]
4. Nesbitt, H.W.; Young, G.M. Foramtion and Diagenesis of Weathering Profiles. *J. Geol.* **1989**, *97*, 129–147. [[CrossRef](#)]
5. Fralick, P.W.; Kronberg, B.I. Geochemical Discrimination of Clastic Sedimentary Rock Sources. *Sediment. Geol.* **1997**, *113*, 111–124. [[CrossRef](#)]
6. Zimmermann, U.; Heinrich, B. Provenance Analysis and Tectonic Setting of the Ordovician Clastic Deposits in the Southern Puna Basin, NW Argentina. *Sedimentology* **2003**, *50*, 1079–1104. [[CrossRef](#)]
7. Zhang, Y.; Pe-Piper, G.; Piper, D.J.W. Sediment geochemistry as a provenance indicator: Unravelling the cryptic signatures of polycyclic sources, climate change, tectonism and volcanis. *Sedimentology* **2014**, *61*, 383–410. [[CrossRef](#)]
8. Armstrong-Altrin, J.S.; Nagarajan, R.; Balaram, V.; Natalhy-Pineda, O. Petrography and Geochemistry of Sands from the Chachalacas and Veracruz Beach Areas, Western Gulf of Mexico, Mexico: Constraints on Provenance and Tectonic Setting. *J. South Am. Earth Sci.* **2015**, *64*, 199–216. [[CrossRef](#)]
9. Baldermann, A.; Abdullayev, E.; Taghiyeva, Y.; Alasgarov, A.; Javad-Zada, Z. Sediment Petrography, Mineralogy and Geochemistry of the Miocene Islam Da?G Section (Eastern Azerbaijan): Implications for the Evolution of Sediment Provenance, Palaeo-Environment and (Post-)Depositional Alteration Patterns. *Sedimentology* **2020**, *67*, 152. [[CrossRef](#)]
10. Kan, W.; Yang, Z.; Yu, L.; Sun, M. Provenance and Tectonic Setting of Formation of Quaternary Sedimentary Successions from the Songhua River, Northeast China. *Appl. Sci.* **2022**, *12*, 7356. [[CrossRef](#)]
11. Bahlburg, H.; Dobrzinski, N. A Review of the Chemical Index of Alteration (CIA) and Its Application to the Study of Neoproterozoic Glacial Deposits and Climate Transitions. In *The Geological Record of Neoproterozoic Glaciations*; Arnaud, E., Halverson, G.P., Shields-Zhou, G., Eds.; Geological Society of London: London, UK, 2011; pp. 81–92.
12. Adeigbe, O.C.; Jimoh, Y.A. Geochemical Fingerprints; Implication for Provenance, Tectonic and Depositional Settings of Lower Benue Trough Sequence, Southeastern Nigeria. *J. Environ. Earth Sci.* **2013**, *3*, 115–141.
13. Yan, Y.; Xia, B.; Lin, G.; Carter, A.; Hu, X.; Cui, X.; Liu, B.; Yan, P.; Song, Z. Geochemical and Nd Isotope Composition of Detrital Sediments on the North Margin of the South China Sea: Provenance and Tectonic Implications. *Sedimentology* **2007**, *54*, 1–17. [[CrossRef](#)]
14. Ofili, S.; Soesoo, A.; Panova, G.E.; Hints, R.; Hade, S.; Ainsaar, L. Geochemical Reconstruction of the Provenance, Tectonic Setting and Paleoweathering of Lower Paleozoic Black Shales from Northern Europe. *Minerals* **2022**, *12*, 602. [[CrossRef](#)]
15. Ivančič, K.; Trajanova, M.; Skaberne, D.; Šmuc, A. Provenance of the Miocene Slovenj Gradec Basin Sedimentary Fill, Western Central Paratethys. *Sediment. Geol.* **2018**, *375*, 256–267. [[CrossRef](#)]
16. Krissek, L.A.; Kyle, P.R. Geochemical Indicators of Weathering, Cenozoic Palaeoclimates, and Provenance in Fine-Grained Sediments from CRP-3, Victoria Land Basin, Antarctica. *Terra Antarct.* **2000**, *8*, 561–568.
17. Royden, H.L.; Horvath, F. Introduction to the Pannonian Region. In *The Pannonian Basin: A Study in Basin Evolution*; Royden, H.L., Horvath, F., Eds.; American Association of Petroleum Geologists: Tulsa, OK, USA, 1988; ISBN 978-1-62981-134-5.
18. Ustaszewski, K.; Schmid, S.M.; Fügenschuh, B.; Tischler, M.; Kissling, E.; Spakman, W. A Map-View Restoration of the Alpine-Carpathian-Dinaridic System for the Early Miocene. *Swiss J. Geosci.* **2008**, *101*, 273–294. [[CrossRef](#)]
19. Schmid, S.M.; Fügenschuh, B.; Kounov, A.; Maženco, L.; Nievergelt, P.; Oberhänsli, R.; Pleuger, J.; Schefer, S.; Schuster, R.; Tomljenović, B.; et al. Tectonic Units of the Alpine Collision Zone between Eastern Alps and Western Turkey. *Gondwana Res.* **2020**, *78*, 308–374. [[CrossRef](#)]
20. Schmid, S.M.; Fügenschuh, B.; Kissling, E.; Schuster, R. Tectonic Map and Overall Architecture of the Alpine Orogen. *Eclogae Geol. Helv.* **2004**, *97*, 93–117. [[CrossRef](#)]
21. Tomljenović, B.; Csontos, L. Neogene-Quaternary Structures in the Border Zone between Alps, Dinarides and Pannonian Basin (Hrvatsko Zgorje and Karlovac Basins, Croatia). *Int. J. Earth Sci.* **2001**, *90*, 560–578. [[CrossRef](#)]
22. Handy, M.R.; Ustaszewski, K.; Kissling, E. Reconstructing the Alps–Carpathians–Dinarides as a Key to Understanding Switches in Subduction Polarity, Slab Gaps and Surface Motion. *Int. J. Earth Sci.* **2014**, *104*, 1–26. [[CrossRef](#)]
23. Kováč, M.; Halásová, E.; Hudáčková, N.; Holcová, K.; Hyžný, M.; Jamrich, M.; Ruman, A. Towards Better Correlation of the Central Paratethys Regional Time Scale with the Standard Geological Time Scale of the Miocene Epoch. *Geol. Carpathica* **2018**, *69*, 283–300. [[CrossRef](#)]
24. Kováč, M.; Hudáčková, N.; Halásová, E.; Kováčová, M.; Holcová, K.; Oszczypko-Clowes, M.; Báldi, K.; Less, G.; Nagymarosy, A.; Ruman, A.; et al. The Central Paratethys Palaeoceanography: A Water Circulation Model Based on Microfossil Proxies, Climate, and Changes of Depositional Environment. *Acta Geol. Slovaca* **2017**, *9*, 75–114.
25. Grizelj, A.; Peh, Z.; Tiblja, D. Mineralogical and Geochemical Characteristics of Miocene Pelitic Sedimentary Rocks from the South-Western Part of the Pannonian Basin System (Croatia): Implications for Provenance Studies. *Geosci. Front.* **2017**, *8*, 65–80. [[CrossRef](#)]
26. Ali, A.; Wagreeich, M. Geochemistry, Environmental and Provenance Study of the Middle Miocene Leitha Limestones (Central Paratethys). *Geol. Carpathica* **2017**, *68*, 248–268. [[CrossRef](#)]
27. Slovenec, D.; Lugovic, B. Amphibole Gabbroic Rocks from the Mt. Medvednica Ophiolite Mélange (NW Croatia): Geochemistry and Tectonic Setting. *Geol. Carpathica* **2008**, *59*, 277–293.
28. Grizelj, A.; Tibljaš, D.; Kovačić, M. Mineralogy and Geochemistry of Upper Miocene Pelitic Sediments of the Zagorje Basin (Croatia): Implication for Evolution of the Pannonian Basin. *Geol. Carpathica* **2007**, *58*, 263–276.

29. Fodor, L.; Csontos, L.; Bada, G.; Györfi, I.; Benkovics, L. Tertiary Tectonic Evolution of the Pannonian Basin System and Neighbouring Orogens: A New Synthesis of Palaeostress Data. *Geol. Soc. Lond. Spec. Publ.* **1999**, *156*, 295–334. [[CrossRef](#)]
30. Huisman, R.S.; Podladchikov, Y.Y.; Cloetingh, S.A.P.L. The Pannonian Basin: Dynamic Modelling of the Transition from Passive to Active Rifting. *Stephan Mueller Spec. Publ. Ser.* **2001**, *3*, 41–63. [[CrossRef](#)]
31. Fodor, L.; Bada, G.; Csillag, G.; Horváth, E.; Ruzsiczay-Rüdiger, Z.; Palotás, K.; Síkhegyi, F.; Timár, G.; Cloetingh, S.; Horváth, F. An Outline of Neotectonic Structures and Morphotectonics of the Western and Central Pannonian Basin. *Tectonophysics* **2005**, *410*, 15–41. [[CrossRef](#)]
32. Tari, G.; Báldi, T.; Báldi-Beke, M. Paleogene Retroarc Flexural Basin beneath the Neogene Pannonian Basin: A Geodynamic Model. *Tectonophysics* **1993**, *226*, 433–455. [[CrossRef](#)]
33. Lorinczi, P.; Houseman, G. Geodynamical Models of Lithospheric Deformation, Rotation and Extension of the Pannonian Basin of Central Europe. *Tectonophysics* **2010**, *492*, 73–87. [[CrossRef](#)]
34. Csontos, L.; Nagymarosy, A. The Mid-Hungarian Line: A Zone of Repeated Tectonic Inversions. *Tectonophysics* **1998**, *297*, 51–71. [[CrossRef](#)]
35. Froitzheim, N.; Schmid, S.M. Orogenic Processes in the Alpine Collision Zone. *Swiss J. Geosci.* **2008**, *101*, 7–9. [[CrossRef](#)]
36. Sachsenhofer, R.F.; Jelen, B.; Hasenhüttl, C.; Dunkl, I.; Rainer, T. Thermal History of Tertiary Basins in Slovenia (Alpine-Dinaride-Pannonian Junction). *Tectonophysics* **2001**, *334*, 77–99. [[CrossRef](#)]
37. Pavelić, D.; Kovačić, M. Sedimentology and Stratigraphy of the Neogene Rift-Type North Croatian Basin (Pannonian Basin System, Croatia): A Review. *Mar. Pet. Geol.* **2018**, *91*, 455–469. [[CrossRef](#)]
38. Ivančić, K.; Trajanova, M.; Ćorić, S.; Rožič, B.; Šmuc, A. Miocene Paleogeography and Biostratigraphy of the Slovenj Gradec Basin: A Marine Corridor between the Mediterranean and Central Paratethys. *Geol. Carpathica* **2018**, *69*, 528–544. [[CrossRef](#)]
39. Vlček, T.; Šarinová, K.; Rybár, S.; Hudáčková, N.; Jamrich, M.; Šujan, M.; Franců, J.; Nováková, P.; Sliva, L.; Kováč, M.; et al. Paleoenvironmental Evolution of Central Paratethys Sea and Lake Pannon during the Cenozoic. *Palaeogeogr. Palaeoclimatol. Palaeoecol.* **2020**, *559*, 109892. [[CrossRef](#)]
40. Hohenegger, J.; Coric, S.; Wagreich, M. Timing of the Middle Miocene Badenian Stage of the Central Paratethys. *Geol. Carpathica* **2014**, *65*, 55–66. [[CrossRef](#)]
41. Rögl, F. Mediterranean and Paratethys. Facts and Hypotheses of an Oligocene to Miocene Paleogeography (Short Overview). *Geol. Carpathica* **1999**, *50*, 339–349.
42. Mandić, O.; Kurečić, T.; Neubauer, T.A.; Harzhauser, M. Stratigraphic and Paleogeographic Significance of Lacustrine Mollusks from the Pliocene Viviparus Beds in Central Croatia. *Geol. Croat.* **2015**, *68*, 179–207. [[CrossRef](#)]
43. Piller, W.E.; Harzhauser, M.; Mandic, O. Miocene Central Paratethys Stratigraphy—Current Status and Future Directions. *Stratigraphy* **2007**, *4*, 151–168. [[CrossRef](#)]
44. Rögl, F. Palaeogeographic Considerations for Mediterranean and Paratethys Seaways (Oligocene to Miocene). *Ann. Naturhistorischen Mus. Wien* **1998**, *99A*, 279–310.
45. Vrabec, M.; Pavlovic Preseren, P.; Stopar, B. GPS Study (1996–2002) of Active Deformation along the Paeradiatic Fault System in Northeastern Slovenia: Tectonic Model. *Geol. Carpathica* **2006**, *57*, 57–65.
46. Mlakar, I. On the Age of the Lower Part of Pseudozilian Beds in the Region of Cerknjo. *Geologija* **1980**, *23*, 173–176.
47. Premru, U. *Osnovna Geološka Karta SFRJ 1:100.000. Tolmač Lista Ljubljana*; Zvezni Geološki Zavod: Belgrade, Serbia, 1983.
48. Janák, M.; Froitzheim, N.; Vrabec, M.; Krogh Ravna, E.J.; De Hoog, J.C.M. Ultrahigh-Pressure Metamorphism and Exhumation of Garnet Peridotite in Pohorje, Eastern Alps. *J. Metamorph. Geol.* **2006**, *24*, 19–31. [[CrossRef](#)]
49. Frisch, W.; Dunkl, I.; Kuhlemann, J. Post-Collisional Orogen-Parallel Large-Scale Extension in the Eastern Alps. *Tectonophysics* **2000**, *327*, 239–265. [[CrossRef](#)]
50. Kralj, P. Potassium Feldspars in the Smrekovec Volcaniclastic Rocks—A Byproduct of the Reaction from Laumontite to Analcime. *Geologija* **2001**, *44*, 325–330. [[CrossRef](#)]
51. Vlahović, I.; Tišljarić, J.; Velić, I.; Matičec, D. Evolution of the Adriatic Carbonate Platform: Palaeogeography, Main Events and Depositional Dynamics. *Palaeogeogr. Palaeoclimatol. Palaeoecol.* **2005**, *220*, 333–360. [[CrossRef](#)]
52. Placer, L. Principles of the Tectonic Subdivision of Slovenia. *Geologija* **2008**, *51*, 205–217. [[CrossRef](#)]
53. Vrabec, M. *Govški Peščenjak v Profilu Doblič*; Univerza v Ljubljani: Ljubljana, Slovenia, 2000.
54. Gašparič, R.; Križnar, M. Early Miocene Decapod Retropluma Slovenica Gašparič & Hyžný, 2014 from Govce Beds of Tunjice Hills (Central Slovenia). *Geologija* **2017**, *60*, 77–85. [[CrossRef](#)]
55. Kuščer, D. Zagorski Terciar. *Geologija* **1967**, *10*, 5–85.
56. Avanić, R.; Pavelić, D.; Pécskay, Z.; Miknić, M.; Tibljaš, D.; Wacha, L. Tidal Deposits in the Early Miocene Central Paratethys: The Vučji Jarek and Čemernica Members of the Macelj Formation (NW Croatia). *Geol. Croat.* **2021**, *74*, 41–56. [[CrossRef](#)]
57. Haq, B.U.; Hardenbol, J.; Vail, P.R. Mesozoic and Cenozoic Chronostratigraphy and Cycles of Sea Level Changes. In *Sea-Level Changes—An Integrated Approach*; Wilgus, C.K., Hastings, B.S., Kendall, C., Posamentie, H., Ross, C.A., Van Wagoner, J., Eds.; SEPM Special Publications: Tulsa, OK, USA, 1988; Volume 42, pp. 71–108. [[CrossRef](#)]
58. Holcová, K.; Doláková, N.; Nehyba, S.; Vacek, F. Timing of Langhian Bioevents in the Carpathian Foredeep and North East Pannonian Basin in Relation to Oceanographic, Tectonic and Climatic Processes. *Geol. Q.* **2018**, *62*, 3–17.
59. Mikuž, V. Miocene Sea Mussels from Neighbourhood of Stolnik in Tunjisko Gričevje (Tunjice Hills), Slovenia. *Geologija* **2009**, *52*, 153–164. [[CrossRef](#)]

60. Vrabec, M. Strukturna Analiza Cone Savskega Preloma Med Trstenikom in Stahovico. Ph.D. Thesis, Univerza v Ljubljani, Ljubljana, Slovenia, 2001.
61. Atanackov, J.; Jamšek Rupnik, P.; Jež, J.; Celarc, B.; Novak, M.; Milanič, B.; Markelj, A.; Bavec, M.; Kastelic, V. Database of Active Faults in Slovenia: Compiling a New Active Fault Database at the Junction Between the Alps, the Dinarides and the Pannonian Basin Tectonic Domains. *Front. Earth Sci.* **2021**, *9*, 604388. [CrossRef]
62. Kresevič, A. Sedimentologija in Tektonska Struktura Srednjemiocenskih Plasti v Tunjiškem Gričevju. Bachelor's Thesis, University of Ljubljana, Ljubljana, Slovenia, 2016. Available online: <https://repozitorij.uni-lj.si/IzpisGradiva.php?lang=slv&id=87833> (accessed on 3 January 2024).
63. Rojnik, A. Sedimentološke in Petrološke Značilnosti Klastičnih Kamnin Laške Formacije v Profilu Doblič. Bachelor's Thesis, University of Ljubljana, Ljubljana, Slovenia, 2015. Available online: <https://repozitorij.uni-lj.si/IzpisGradiva.php?lang=eng&id=73303> (accessed on 3 January 2024).
64. Zachos, J.; Pagani, M.; Sloan, L.; Thomas, E.; Billups, K. Trends, Rhythms, and Aberrations in Global Climate 65 Ma to Present. *Science* **2001**, *292*, 686–693. [CrossRef] [PubMed]
65. Nesbitt, H.W.; Young, G.M. Prediction of Some Weathering Trends of Plutonic and Volcanic Rocks Based on Thermodynamic and Kinetic Considerations. *Geochim. Cosmochim. Acta* **1984**, *48*, 1523–1534. [CrossRef]
66. Roser, B.P.; Korsch, R.J. Provenance Signatures of Sandstone-Mudstone Suites Determined Using Discriminant Function of Major-Element Data. *Chem. Geol.* **1988**, *67*, 119–139. [CrossRef]
67. Oni, S.O.; Olatunji, A.S.; Ehinola, O.A. Determination of Provenance and Tectonic Settings of Niger Delta Clastic Facies Using Well-Y, Onshore Delta State, Nigeria. *J. Geochem.* **2014**, *2014*, 960139. [CrossRef]
68. Bhatia, M.R. Plate Tectonics and Geochemical Composition of Sandstone. *J. Geol.* **1983**, *91*, 611–627. [CrossRef]
69. Herron, M.M. Geochemical Classification of Terrigenous Sands and Shales from Core or Log Data. *SEPM J. Sediment. Res.* **1988**, *58*, 820–829. [CrossRef]
70. Hu, J.; Li, Q.; Fang, N.; Yang, J.; Ge, D. Geochemistry Characteristics of the Low Permian Sedimentary Rocks from Central Uplift Zone, Qiangtang Basin, Tibet: Insights into Source-Area Weathering, Provenance, Recycling, and Tectonic Setting. *Arab. J. Geosci.* **2015**, *8*, 5373–5388. [CrossRef]
71. Fedo, C.M.; Nesbitt, H.W.; Young, G.M. Unravelling the Effects of Potassium Metasomatism in Sedimentary Rocks and Paleosols, with Implications for Paleoweathering Conditions and Provenance. *Geology* **1995**, *23*, 921–924. [CrossRef]
72. Tawfik, H.A.; Ghandour, I.M.; Maejima, W.; Armstrong-Altrin, J.S.; Abdel-Monem, T.; Abdel-Hameed, A.-M.T. Petrography and Geochemistry of the Siliciclastic Araba Formation (Cambrian), East Sinai, Egypt: Implications for Provenance, Tectonic Setting and Source Weathering. *Geol. Mag.* **2015**, *154*, 1–23. [CrossRef]
73. Harzhauser, M.; Piller, W.E. Benchmark Data of a Changing Sea—Palaeogeography, Palaeobiogeography and Events in the Central Paratethys during the Miocene. *Palaeogeogr. Palaeoclimatol. Palaeoecol.* **2007**, *253*, 8–31. [CrossRef]
74. Weaver, C.E. *Clays, Muds, and Shales*; Elsevier Science Publishers B.V.: Amsterdam, The Netherlands, 1989.
75. Kováčová, M.; Doláková, N.; Kovac, M. Miocene Vegetation Pattern and Climate Change in the Northwestern Central Paratethys Domain (Czech and Slovak Republic). *Geol. Carpathica* **2011**, *62*, 251–266. [CrossRef]
76. Kováčová, M.; Sitár, V. Early Miocene Flora of the South Slovakian Basin. *Acta Palaeobot.* **2007**, *47*, 163–181.
77. Karami, M.P.; de Leeuw, A.; Krijgsman, W.; Meijer, P.T.; Wortel, M.J.R. The Role of Gateways in the Evolution of Temperature and Salinity of Semi-Enclosed Basins: An Oceanic Box Model for the Miocene Mediterranean Sea and Paratethys. *Glob. Planet. Chang.* **2011**, *79*, 73–88. [CrossRef]
78. Pavelić, D.; Kovačić, M.; Banak, A.; Jiménez-Moreno, G.; Marković, F.; Pikelj, K.; Vranjković, A.; Premužak, L.; Tibljaš, D.; Belak, M. Early Miocene European Loess: A New Record of Aridity in Southern Europe. *Geol. Soc. Am. Bull.* **2016**, *128*, 110–121. [CrossRef]
79. Kováč, M.; Andreyeva-Grigorovich, A.; Bajraktarević, Z.; Brzobohatý, R.; Filipescu, S.; Fodor, L.; Harzhauser, M.; Nagymarosy, A.; Oszczytko, N.; Pavelić, D.; et al. Badenian Evolution of the Central Paratethys Sea: Paleogeography, Climate and Eustatic Sea-Level Changes. *Geol. Carpathica* **2007**, *58*, 579–606.
80. Abreu, V.S.; Haddad, G.A. Glacioeustatic Fluctuations: The Mechanism Linking Stable Isotope Events and Sequence Stratigraphy from the Early Oligocene to Middle Miocene. In *Mesozoic and Cenozoic Sequence Stratigraphy of European Basins*; Graciansky, C.-P., Hardenbol, J., Jacquin, T., Vail, P.R., Eds.; SEPM Special Publications: Tulsa, OK, USA, 1998; Volume 60, pp. 245–260.
81. Alqahtani, F.; Khalil, M. Geochemical Analysis for Evaluating the Paleoweathering, Paleoclimate, and Depositional Environments of the Siliciclastic Miocene-Pliocene Sequence at Al-Rehaili Area, Northern Jeddah, Saudi Arabia. *Arab. J. Geosci.* **2021**, *14*, 239. [CrossRef]
82. Mustafa, R.K. Geochemical Application in Unraveling Paleoweathering, Provenance and Environmental Setting of the Shale from Chia Gara Formation, Kurdistan Region. *Iraqi Geol. J.* **2020**, *53*, 90–116. [CrossRef]
83. Dress, L.R.; Wilding, L.P.; Smeck, N.E.; Senkay, A.L. Silica in Soils: Quartz and Disordered Silica Polymorphs. In *Minerals in Soil Environments*; Dixon, J.B., Ed.; Soil Science Society of America: Madison, WI, USA, 1989; pp. 913–965.
84. Tišljar, J. *Sedimentologija Klastičnih i Silicijskih Taložina*; Velić, I., Ed.; Institut z.; Nacionalna i sveučilišna knjižnica-Zagreb: Zagreb, Croatia, 2004.
85. McKosky, J.A. Quartz in Provenance Examination. Master's Thesis, Michigan State University, Lansing, MI, USA, 1975.
86. Trajanova, M.; Pecskay, Z.; Itaya, T. K-Ar Geochronology and Petrography of the Miocene Pohorje Mountains Batholith (Slovenia). *Geol. Carpathica* **2008**, *59*, 247–260.

87. Janák, M.; Froitzheim, N.; Lupták, B.; Vrabec, M.; Ravna, E.J.K. First Evidence for Ultrahigh-Pressure Metamorphism of Eclogites in Pohorje, Slovenia: Tracing Deep Continental Subduction in the Eastern Alps. *Tectonics* **2004**, *23*, 1–10. [[CrossRef](#)]
88. White, B.W. Speleothems. In *Encyclopedia of Caves*; White, W.B., Culver, D.C., Pipan, T., Eds.; Academic Press: Cambridge, MA, USA, 2019; pp. 1006–1017, ISBN 978-0-12-814124-3.
89. Sulpis, O.; Jeansson, E.; Dinauer, A.; Lauvset, S.K.; Middelburg, J.J. Calcium Carbonate Dissolution Patterns in the Ocean. *Nat. Geosci.* **2021**, *14*, 423–428. [[CrossRef](#)]
90. Piller, W.E.; Harzhauser, M. The Myth of the Brackish Sarmatian Sea. *Terra Nova* **2005**, *17*, 450–455. [[CrossRef](#)]
91. Pettijohn, F.J.; Potter, P.E.; Siever, R. *Sand and Sandstone*; Springer: New York, NY, USA, 1972.
92. Hinterlechner-Ravnik, A. Zeleni Skrilavci Kranjske Rebri. *Geologija* **1978**, *21*, 245–254.
93. Trajanova, M. Uvod v Magmatske Kamnine Slovenije = Introduction to Igneous Rocks of Slovenia. In *Geologija Slovenije = The Geology of Slovenia*; Pleničar, M., Ogorelec, B., Novak, M., Eds.; Geološki Zavod Slovenije: Ljubljana, Slovenia, 2009; pp. 467–468. ISBN 978-961-6498-24-1.
94. Ney, R.; Burzewski, W.; Bachleda, T.; Górecki, W.; Jakóbczak, K.; Supczyński, K. Outline of Paleogeography and Evolution of Lithology and Facies of Miocene Layers on the Car-Pathian Foredeep. *Prace Geol.* **1974**, *82*, 1–65.
95. Săndulescu, M. Cenozoic Tectonic History of the Carpathians. In *The Pannonian Basin—A Study in Basin Evolution*; Royden, L., Horvath, F., Eds.; The American Association of Petroleum Geologists and The Hungarian Geological Society, AAPG: Tulsa, OK, USA, 1988; pp. 17–26.
96. Meunier, A.; Caner, L.; Hubert, F.; El Albani, A.; Pret, D. The Weathering Intensity Scale (WIS): An Alternative Approach of the Chemical Index of Alteration (CIA). *Am. J. Sci.* **2013**, *313*, 113–143. [[CrossRef](#)]
97. Berner, R.A. Sedimentary Pyrite Formation: An Update. *Geochim. Cosmochim. Acta* **1984**, *48*, 605–615. [[CrossRef](#)]
98. Čorić, S.; Pavelić, D.; Rögl, F.; Mandić, O.; Vrabec, S. Revised Middle Miocene Datum for Initial Marine Flooding of North Croatian Basins (Pannonian Basin System, Central Paratethys). *Geol. Croat.* **2009**, *62*, 31–43. [[CrossRef](#)]
99. Girty, G.; Ridge, D.L.; Knaack, C.; Johnson, D.; Al-Riyami, R.K. Provenance and Depositional Setting of Paleozoic Chert and Argillite, Sierra Nevada, California. *J. Sediment. Res.* **1996**, *66*, 107–118. [[CrossRef](#)]
100. Garcia, D.; Moutte, J. Sedimentary Fractionations between Al, Ti, and Zr and the Genesis of Strongly Peraluminous Granites. *J. Geol.* **1994**, *102*, 411–422. [[CrossRef](#)]
101. Nagarajan, R.; Armstrong-Altrin, J.S.; Kessler, F.L.; Hidalgo-Moral, E.L.; Dodge-Wan, D.; Taib, N.I. Provenance and Tectonic Setting of Miocene Siliciclastic Sediments, Sibuti Formation, Northwestern Borneo. *Arab. J. Geosci.* **2015**, *8*, 8549–8565. [[CrossRef](#)]
102. Spalletti, L.A.; Limarino, C.O.; Piñol, F.C. Petrology and Geochemistry of Carboniferous Siliciclastics from the Argentine Frontal Cordillera: A Test of Methods for Interpreting Provenance and Tectonic Setting. *J. South Am. Earth Sci.* **2012**, *36*, 32–54. [[CrossRef](#)]
103. Absar, N.; Sreenivas, B. Petrology and Geochemistry of Greywackes of the ~1.6 Ga Middle Aravalli Supergroup, Northwest India: Evidence for Active Margin Processes. *Int. Geol. Rev.* **2015**, *57*, 134–158. [[CrossRef](#)]
104. Zhou, L.; Frii, H.; Poulsen, M.L.K. Geochemical Evaluation of the Late Paleocene and Early Eocene Shales in Siri Canyon, Danish-Norwegian Basin. *Mar. Pet. Geol.* **2015**, *61*, 111–122. [[CrossRef](#)]
105. Hayashi, K.I.; Fujisawa, H.; Holland, H.D.; Ohmoto, H. Geochemistry of ~1.9 Ga Sedimentary Rocks from Northeastern Labrador, Canada. *Geochim. Cosmochim. Acta* **1997**, *61*, 4115–4137. [[CrossRef](#)]
106. Allaby, M. *A Dictionary of Earth Sciences*; Oxford University Press: Oxford, UK, 2008; ISBN 9780199211944.
107. Vrabec, M.; Fodor, L. Late Cenozoic Tectonics of Slovenia: Structural Styles At the Northeastern Corner of the Adriatic Microplate. In *The Adria Microplate: GPS Geodesy, Tectonics and Hazards*; Pinter, N., Grenczy, G., Weber, J., Stein, S., Medak, D., Eds.; Nato Science Series IV: Earth and Environmental Sciences (NAIV); Springer: Dordrecht, The Netherlands, 2006; Volume 61, pp. 151–168. [[CrossRef](#)]
108. Fodor, L.; Jelen, B.; Dragomir, S.; Vrabec, M. Miocene-Pliocene Tectonic Evolution of the Slovenian Periadriatic Fault: Implications for Alpine-Carpathian Extrusion Models. *Tectonics* **1998**, *17*, 690–709. [[CrossRef](#)]
109. Gale, E.M.; Rupnik, P.J.; Trajanova, M.; Gale, L.; Bavec, M.; Anselmetti, F.S.; Šmuc, A. Provenance and Morphostratigraphy of the Pliocene-Quaternary Sediments in the Celje and Drava-Ptuj Basins (Eastern Slovenia). *Geologija* **2019**, *62*, 189–218. [[CrossRef](#)]
110. Bistricic, A.; Jenko, K. Area No. 224 B1: Transtethyan Trench “Corridor”, YU. In *Neogene of the Mediterranean Tethys and Paratethys. Stratigraphic Correlation Tables and Sediment Distribution Maps*; Steininger, F.F., Senes, J., Kleemann, K., Rögl, F., Eds.; University of Vienna: Vienna, Austria, 1985; Volume 1, pp. 72–73.
111. Bartol, M.; Mikuž, V.; Horvat, A. Palaeontological Evidence of Communication between the Central Paratethys and the Mediterranean in the Late Badenian/Early Serravalian. *Palaeogeogr. Palaeoclimatol. Palaeoecol.* **2014**, *394*, 144–157. [[CrossRef](#)]
112. Dobnikar, M.; Zupančič, N. Triasne Globočnine Železnokapelske Magmatske Cone. In *Geologija Slovenije = The Geology of Slovenia*; Pleničar, M., Ogorelec, B., Novak, M., Eds.; Geološki Zavod Slovenije: Ljubljana, Slovenia, 2009; pp. 473–478.
113. Dobnikar, M.; Dolenc, T.; Činčuhant, B.; Zupančič, N. Magmatic Rocks of the Karavanke Granitic Massif, Slovenia. *Geologija* **2000**, *45*, 55–59. [[CrossRef](#)]
114. Kralj, P.; Celarc, B. Shallow Intrusive Volcanic Rocks on Mt. Raduha, Savinja-Kamnik Alps, Northern Slovenia. *Geologija* **2002**, *45*, 247–253. [[CrossRef](#)]
115. Štrucl, I. Stratigrafske in Tektonske Razmere v Vzhodnem Delu Severnih Karavank. *Geologija* **1970**, *13*, 5–20.
116. Schmid, S.M.; Bernoulli, D.; Fügenschuh, B.; Matenco, L.; Schefer, S.; Schuster, R.; Tischler, M.; Ustaszewski, K. The Alpine-Carpathian-Dinaridic Orogenic System: Correlation and Evolution of Tectonic Units. *Swiss J. Geosci.* **2008**, *101*, 139–183. [[CrossRef](#)]

117. Kutterolf, S.; Diener, R.; Schacht, U.; Krawinkel, H. Provenance of the Carboniferous Hochwipfel Formation (Karawanken Mountains, Austria/Slovenia)—Geochemistry versus Petrography. *Sediment. Geol.* **2008**, *203*, 246–266. [[CrossRef](#)]
118. Stampfli, G.M.; Borel, G.D. A Plate Tectonic Model for the Paleozoic and Mesozoic Constrained by Dynamic Plate Boundaries and Restored Synthetic Oceanic Isochrones. *Earth Planet. Sci. Lett.* **2002**, *196*, 17–33. [[CrossRef](#)]
119. Robertson, A.H.F.; Dixon, J.E. Introduction: Aspects of the Geological Evolution of the Eastern Mediterranean. *Geol. Soc. Lond. Spec. Publ.* **1996**, *17*, 1–74. [[CrossRef](#)]
120. Dercourt, J.; Suczek, C.A.; Vrielynck, B. (Eds.) *Atlas Tethys Palaeoenvironmental Maps: Explanatory Notes*; Gauthier-Villars: Paris, France, 1993; 307p.
121. Kovács, I.; Szabó, C. Middle Miocene Volcanism in the Vicinity of the Middle Hungarian Zone: Evidence for an Inherited Enriched Mantle Source. *J. Geodyn.* **2008**, *45*, 1–17. [[CrossRef](#)]
122. Armstrong-Altrin, J.S.; Verma, S.P. Critical Evaluation of Six Tectonic Setting Discrimination Diagrams Using Geochemical Data of Neogene Sediments from Known Tectonic Settings. *Sediment. Geol.* **2005**, *177*, 115–129. [[CrossRef](#)]
123. Schmid, S.M.; Pfiffner, O.A.; Froitzheim, N.; Schonborn, G.; Kissling, E. Geophysical-Geological Transect and Tectonic Evolution of the Swiss-Italian Alps. *Tectonics* **1996**, *15*, 1036–1064. [[CrossRef](#)]
124. Ratschbacher, L.; Frisch, W.; Hans-Gert, L.; Merle, O. Lateral Extrusion in the Eastern Alps, Part 2: Structural Analysis. *Tectonics* **1991**, *10*, 245–256. [[CrossRef](#)]
125. Frisch, W.; Kuhlemann, J.; Dunkl, I.; Brügel, A. Palinspastic Reconstruction and Topographic Evolution of the Eastern Alps during Late Tertiary Tectonic Extrusion. *Tectonophysics* **1998**, *297*, 1–15. [[CrossRef](#)]
126. Placer, L. Contribution to the Macrotectonic Subdivision of the Border Region between Southern Alps and External Dinarides. *Geologija* **1999**, *41*, 223–255. [[CrossRef](#)]
127. Tari, G. Evolution of the Northern and Western Dinarides: A Tectonostratigraphic Approach. In *Proceedings of the Continental Collision and the Tectonosedimentary Evolution of Forelands*; Bertotti, K., Schulmann, K., Cloething, S.A.P.L., Eds.; EGU Stephan Mueller Publication Series; European Geosciences Union: Munich, Germany, 2002; pp. 223–236. [[CrossRef](#)]
128. Horváth, F.; Royden, H.L. Mechanism for the Formation of the Intra-Carpathian Basins: A Review. *Earth Sci. Rev.* **1981**, *1*, 307–316.
129. Horváth, F. Phases of Compression during the Evolution of the Pannonian Basin and Its Bearing on Hydrocarbon Exploration. *Mar. Pet. Geol.* **1995**, *12*, 837–844. [[CrossRef](#)]
130. Ebner, F.; Sachsenhofer, R.F. Palaeogeography, Subsidence and Thermal History of the Neogene Styrian Basin (Pannonian Basin System, Austria). *Tectonophysics* **1995**, *242*, 133–150. [[CrossRef](#)]
131. Royden, H.L. Late Cenozoic Tectonics of the Pannonian Basin System. In *The Pannonian Basin: A Study in Basin Evolution*; Royden, H.L., Horváth, F., Eds.; American Association of Petroleum Geologists: Tulsa, OK, USA, 1988; pp. 27–48.
132. Kováč, M.; Nagymarosy, A.; Oszczytko, N.; Csontos, L.; Slaczka, A.; Marunteanu, M.; Matenco, L.; Marton, E. Palinspastic Reconstruction of the Carpathian-Pannonian Region during the Miocene. In *Geodynamic Development of the Western Carpathians*; Rakús, M., Ed.; Geological Survey of Slovak Republic: Bratislava, Slovakia, 1998; pp. 189–217.

Disclaimer/Publisher’s Note: The statements, opinions and data contained in all publications are solely those of the individual author(s) and contributor(s) and not of MDPI and/or the editor(s). MDPI and/or the editor(s) disclaim responsibility for any injury to people or property resulting from any ideas, methods, instructions or products referred to in the content.